NAVWEPS REPORT 8528
NOTS TP 3529
COPY

WIND-TUNNEL TESTS ON A POROUS BODY WITH SUCTION

(U)

by

T. G. Lang
and
H. V. L. Patrick

Research Department

ABSTRACT. Tests were performed in a 7-by-10-foot wind tunnel to determine the drag characteristics of a full-scale, porous-shelled torpedo model with suction applied to three internal chambers. The model was a Reichardt body of revolution having a nearly uniform pressure distribution with a fineness ratio of 8:1 and a diameter of 12 3/4 inches. The drag was measured by means of six boundary-layer rakes located 91 inches from the nose. The test data were obtained at Reynolds numbers up to 12×10^6, the turbulence limit of the wind tunnel. (UNCLASSIFIED)

U.S. NAVAL ORDNANCE TEST STATION

China Lake, California

December 1964

U. S. NAVAL ORDNANCE TEST STATION
AN ACTIVITY OF THE BUREAU OF NAVAL WEAPONS

J. I. HARDY, CAPT., USN
Commander

WM. B. MCLEAN, PH.D.
Technical Director

FOREWORD

For several years, the Research and Underwater Ordnance Departments of the U. S. Naval Ordnance Test Station have been engaged in experimental and theoretical investigations of various methods of drag reduction. One of the more promising methods of drag reduction is boundary-layer control by suction. This report gives the results of wind-tunnel tests on a full-scale porous-fiberglass torpedo model with suction. The tests were conducted in November and December 1962, in a 7-by-10-foot subsonic wind tunnel of the Northrop Corp., Norair Division, Hawthorne, Calif.

The work was funded under Bureau of Naval Weapons Task Assignment RUTO-3E-000/216 1/R009-01-03. This report was reviewed for technical adequacy by J. D. Brooks and H. T. Yerby of the Underwater Ordnance Department.

Released by
GILBERT J. PLAIN,
Acting Head,
Research Department
10 November 1964.

Under authority of
WM. B. McLEAN
Technical Director

NOTS Technical Publication 3529
NAVWEPS Report 8528

Published by	Research Department
Manuscript	P5006/MS-10
Collation	Cover, 20 leaves, abstract cards
First printing	200 numbered copies
Security classification	CONFIDENTIAL
Abstract alone	UNCLASSIFIED
Title alone	UNCLASSIFIED

CONTENTS

NEGATIVE NUMBERS OF ILLUSTRATIONS

Fig. 1 through 32, LHL-P 25386, C; Fig. 33, LHL-P 24125, C; Fig. 34, 35, 36, LHL-P 25386, C; Fig. 37, LHL-P 24172, C; Fig. 38, LHL-P 21178, C; Fig. 39, LHL-P 25386, C.

ACKNOWLEDGMENT

The suggestions by Dr. R. W. Pfenninger, of Norair, in planning the tests are greatly appreciated. Special acknowledgment is due Mr. Lloyd Gross, also of Norair, who, under a NOTS contract, supervised the installation of the model and the acquisition and reduction of the test data. The authors are indebted to A. G. Fabula of the Research Department for preparing Appendix C of this report.

NOMENCLATURE

C_{D_S}	Suction-drag coefficient, $C_{D_S} = C_{D_{SS}} + C_{D_{SM}} = \Sigma C_{Q_a} C_{p_a}$
$C_{D_{SM}}$	Momentum-drag coefficient due to momentum loss of flow in portion of boundary layer sucked through shell, $C_{D_{SM}} = C_{D_S} - C_{D_{SS}}$
$C_{D_{SS}}$	Equivalent-drag coefficient in portion of boundary layer sucked through shell owing to pressure drop across porous shell, $C_{D_{SS}} = \sum \frac{C_{Q_a}^2 R_a U_\infty}{q_\infty} = -\sum C_{Q_a}(C_{p_a} - C_{p_e})$
C_{D_t}	Total drag coefficient, $C_{D_t} = C_{D_W} + C_{D_S} = \frac{\text{Drag}}{q_\infty S}$
C_{D_W}	Wake-drag coefficient measured by wake rakes
C_p	Static-pressure coefficient, $C_p = (p - p_\infty)/q_\infty$
C_{p_a}	Static-pressure coefficient for each chamber
C_{p_e}	Static-pressure coefficient outside shell
C_Q	Suction coefficient for total model, $C_Q = \Sigma C_{Q_a}$
C_{Q_a}	Suction coefficient for each chamber, $C_{Q_a} = Q_a/(U_\infty S)$
ℓ	Reference length of model to wake rakes (7.59 ft)
q_∞	Wind-tunnel dynamic pressure, lb/ft^2, $q_\infty = (1/2)\rho U_\infty^2$
Q_a	Suction-rate quantity for each chamber, ft^3/sec
R	Porous-shell resistivity, psi/fps, $R = \frac{p_e - p_a}{v} = (C_{D_{SS}} q_\infty)/(U_\infty C_Q^2)$
R_ℓ	Reynolds number based on length of model given as chord length, $R_\ell = \rho U_\infty \ell/\mu$
S	Wetted area of body (21.65 ft^2)

U_∞ Free-stream wind-tunnel velocity, ft/sec

v Velocity through porous shell, ft/sec

α Angle of attack of model, deg

μ Tunnel air viscosity, lb sec/ft^2

ν Kinematic viscosity of fluid, ft^2/sec

ρ Tunnel air density, slug/ft^3

INTRODUCTION

Interest in achieving a laminar boundary layer through the use of suction began at the U. S. Naval Ordnance Test Station (NOTS) in the mid-1950's, and resulted in a study that included several advanced torpedo concepts (Ref. 1). Discussions of permeable materials, torpedo body shapes, suction rates, pumping characteristics, criteria for body roughness and waviness, results of sea water clogging tests of permeable materials, and descriptions of various types of free-running and gravity-propelled test vehicles are presented in Ref. 2.

While other methods of drag reduction were considered (Ref. 3 and 4), boundary-layer control by suction was believed to have the greatest potential. If the boundary layer were ideally laminar, torpedo drag would be reduced by a factor of about ten at normal speeds. Considering the pumping power needed to provide the required suction, the loss in volume due to ducting, and the addition of fins, a net-equivalent drag-reduction factor of four was considered conservative. Since torpedo volume is reduced as fuel and power requirements are reduced, the power required to propel the torpedo might be reduced by a factor of six or seven.

To investigate practical aspects of boundary-layer control applied to torpedo design, a study was conducted assuming a net drag-reduction factor of four (Ref. 5). Since the effects of boundary-layer control are theoretically the same in air as in water (assuming no cavitation, gas entrainment, or clogging problems), Ref. 6 is an excellent source of information that summarizes relevant research in air, including Dr. W. Pfenninger's work for the Norair Division of the Northrop Corp.

In 1958, NOTS decided to build a full-scale model of a torpedolike body, composed primarily of a sting-mounted porous shell. This body was to be tested in water at the David Taylor Model Basin (DTMB). A contract was let to the H. I. Thompson Company (HITCO) in Los Angeles, Calif., to fabricate the porous-fiberglass shell. Design of the model's internal structure and other research on the fiberglass material was performed at NOTS, while the sting support and suction pump were designed at DTMB. Difficulties with the fiberglass material were encountered by both NOTS and HITCO because of its lack of uniformity in permeability, strength, surface hardness, and water absorption.

The full-scale 8-foot model was completed during the Fall of 1961 and installed in a towing tank at DTMB. During preliminary tare runs in the spring of 1962, the model shell cracked along its joints and was shipped back to NOTS for replacement. A new shell was built and the model was made ready for testing by November 1962. This time,

however, it was decided to first test the model in a wind tunnel at Northrop because of the relative ease of conducting the tests, observing the model, varying the test parameters, and collecting a large mass of data. Other advantages were the nearness of the tunnel to NOTS, the low turbulence level of the tunnel, the help of highly qualified Northrop personnel in conducting the tests, and the possibility of comparing the NOTS porous-shell model with an existing Northrop slotted-metal model. At the conclusion of these tests, it was apparent that the model shell was not sufficiently porous to permit testing in water. The lack of permeability was apparently caused by spraying the completed model shell with resin in order to harden surface regions where the resin content was undesirably low.

This report presents results of these wind-tunnel tests during November and December 1962. Descriptions of the model, pressure distribution, test setup, and data-reduction procedure are included in Appendixes A and B. Results of theoretical boundary-layer calculations are included in Appendix C.

Test results show fully laminar boundary-layer control. The many problems due to lack of uniformity in the fiberglass material show that more development is required; potentially, however, its fabrication cost is low.

In view of current plans by Northrop to test its slotted-metal body in water, no further development of the fiberglass material or additional tests on the NOTS model are planned at this time.

TOTAL DRAG RESULTS

EFFECT OF REYNOLDS NUMBER

Figure 1 shows the total drag coefficient, C_{D_t}, of the entire shell (up to the wake rakes) plotted against the Reynolds number, R_f, for the NOTS model both with and without suction, as well as test results of the 12-foot Northrop slotted-metal body obtained from Ref. 7. Figure 1 also includes a plot of the NOTS model data (with suction) modified for a change in shell permeability. The modification was made because the porous shell that was tested proved to be less permeable than was necessary.

A significant penalty in drag is obtained when the pressure drop across the porous shell is excessive. The desired pressure drop is around $0.10\ q_\infty$, where q_∞ is the free-stream dynamic pressure. This pressure drop is the minimum that will still provide adequate suction everywhere on the shell despite surface-pressure changes caused by maneuvering, shell waviness, and reasonable variations in shell permeability. The slotted-metal shell used in the Norair tests (Ref. 7) had a pressure drop of $0.05\ q_\infty$, in reasonable agreement with the desired value. The NOTS porous-fiberglass model had a pressure drop of about $1.1\ q_\infty$, rather than the design value of $0.10\ q_\infty$. Since earlier

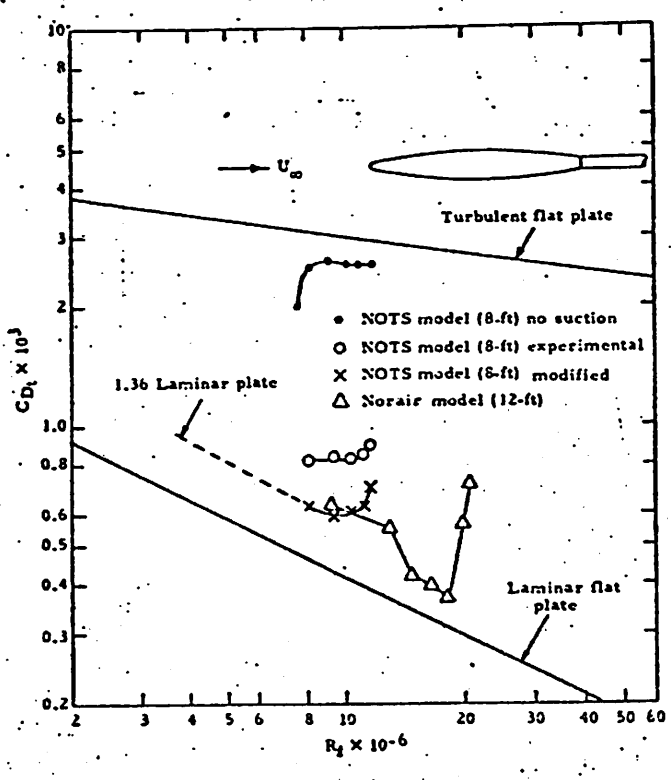

FIG. 1. Total Drag of the NOTS and Northrop Wind-Tunnel Models.

test samples of the porous-fiberglass material had adequate properties, it is reasonable to expect that, with additional development, a porous-fiberglass shell could be obtained with a pressure drop of 0.10 q_∞. Consequently, it is believed that the most reasonable way to present the wind-tunnel results, to permit comparison with the Northrup results and to permit extrapolation to prototype operation, is to modify the shell-pressure drop from 1.1 q_∞ to 0.10 q_∞ in the data presentation.

Three notable facts emerge from Fig. 1:

1. Total drag coefficient of the NOTS model increases markedly beyond $R_f = 12 \times 10^6$, while the Norair model drag coefficient increases markedly beyond about $R_f = 18 \times 10^6$. This difference in Reynolds number ($R_f = fU_\infty/\nu$) indicates that the critical speed of the tunnel is about the same for both models, in view of the greater length of the Norair model. (Critical speed is the point at which tunnel turbulence and vibration cause the model boundary layer to become turbulent.)

2. Test results of both NOTS and Norair models agree up to critical speed, so long as the NOTS model results are modified to allow for shell permeability.

3. Without suction, the boundary layer of the NOTS model is mostly turbulent at the lowest test Reynolds number of 8×10^6, indicating that the transition Reynolds number may have been about the same as for a flat plate in a low-turbulence wind tunnel, namely 3 to 4×10^6.

Using the modified NOTS model figures, the reduction in drag over the test results with no suction is a factor of 4.3 at $R_\ell = 10 \times 10^6$. A prototype torpedo would be operating at about $R_\ell = 50 \times 10^6$; at this point, the drag of a body with suction would be reduced by a factor of about nine from the drag of the same body without suction. Preliminary results of 1962 tests of the Norair model at the NASA variable-density wind tunnel at Ames, Calif., show that laminar flow was obtained up to $R_\ell = 56 \times 10^6$, which corresponds to drag reduction by a factor of nine. This indicates that extrapolation is valid for the Norair model and therefore may be valid for the NOTS model.

EFFECT OF SUCTION RATE

Figures 2 and 3 show the effect of suction rate, C_Q, on the total drag. These results indicate that the effect of suction on total drag coefficient is less critical at the lower Reynolds number, and that the suction coefficient for minimum drag varies from 1.5×10^{-4} up to about 2.1×10^{-4} for $R_\ell = 8$ to 11×10^6.

EFFECT OF ANGLE OF ATTACK

Figure 4 shows the effect of attack angle on minimum drag coefficient to be very small. A detailed inspection of the data indicates that if the model had uniform permeability and no seams, the total drag would go up slightly with increasing angle of attack, rather than reduce slightly as indicated in Fig. 4.

EFFECT OF SUCTION DISTRIBUTION

Figure 5 shows that the total drag up to the rakes, either with or without the shell-permeability correction, remains essentially independent of suction distribution, assuming that the total suction rate is sufficiently high to laminarize the boundary layer. Suction Distribution I is the case where the suction pressure was a constant over the entire model. Suction Distribution II is uniform suction pressure over the first and second compartments, with increased suction pressure over the third compartment. Suction Distribution III is uniform suction pressure over the last two compartments, with less suction pressure over the first compartment. The permeability of the first chamber was 1 2/3 times those of Chambers 2 and 3, both of which had equal permeability. Therefore, Suction Distribution I did not provide uniform suction, even though suction pressure was uniform. (See Appendix A for additional information on permeability and resultant suction distribution for the three suction cases.)

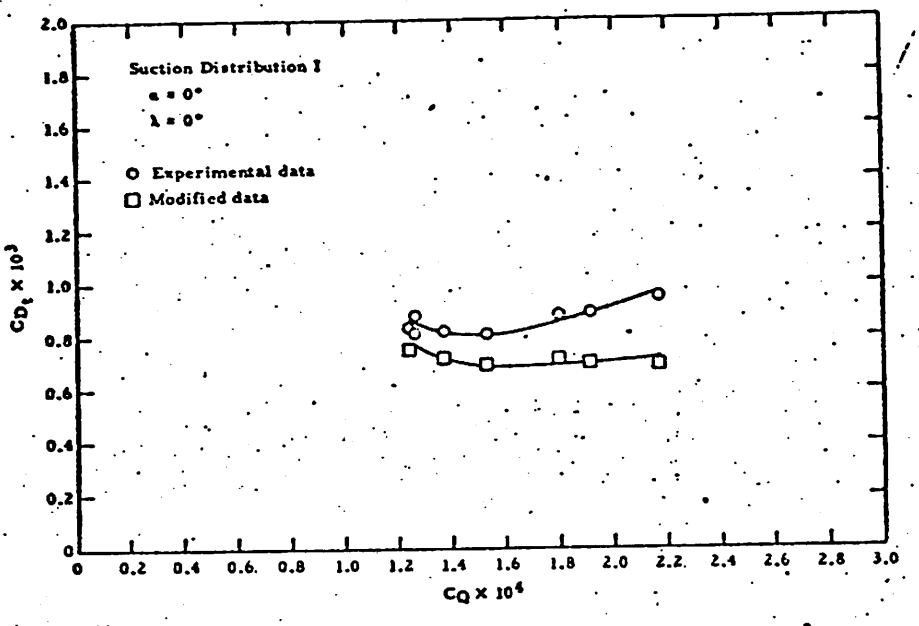

FIG. 2. Effect of Suction Rate on Total Drag; $R_\ell = 8 \times 10^6$.

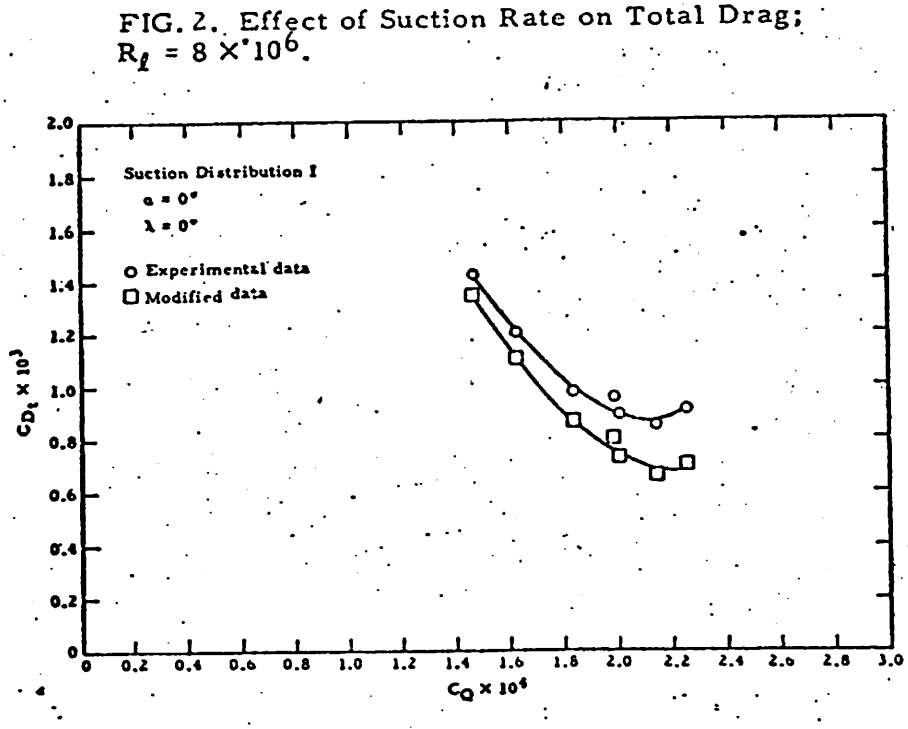

FIG. 3. Effect of Suction Rate on Total Drag; $R_\ell = 11 \times 10^6$.

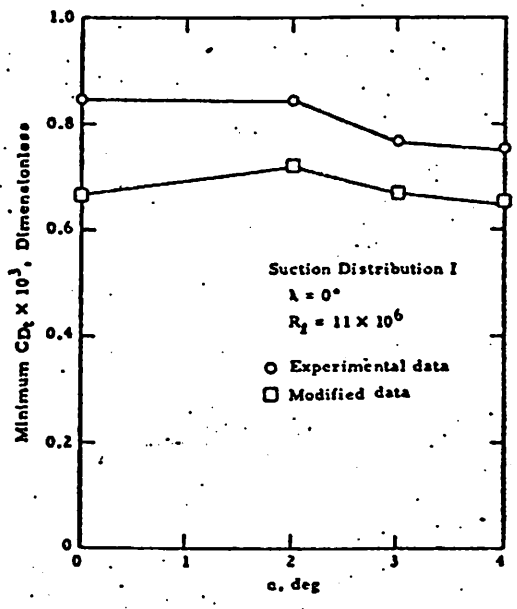

FIG. 4. Total Drag as a Function of Angle of Attack.

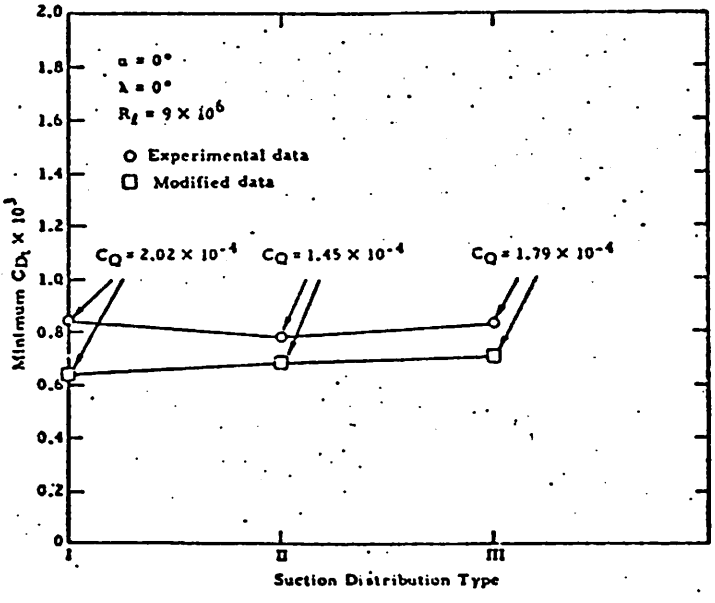

FIG. 5. Effect of Suction Distribution on Total Drag.

COMPONENTS OF TOTAL DRAG

DATA-REDUCTION METHOD

In reducing the data, the total drag of the model, C_{D_t}, is divided into three parts:

1. The wake drag, C_{D_W}, representing the momentum loss in the boundary layer outside the model.
2. $C_{D_{SM}}$, representing the momentum loss of the flow in the portion of the boundary layer that was sucked through the shell.
3. $C_{D_{SS}}$, representing the equivalent drag coefficient produced by the pressure drop across the porous shell.

The sum of $C_{D_{SM}}$ and $C_{D_{SS}}$ is called C_{D_S}, and represents the portion of the total drag coefficient attributable to the action of sucking the fluid inside the shell. The suction drag, C_{D_S}, is calculated as follows: Power loss = $Q\Delta P$, where ΔP is the loss in total pressure from the free-stream condition to the condition inside the model. The equivalent suction drag, then, is the power loss divided by U_∞. The suction drag coefficient equals the suction drag divided by $q_\infty S$. Thus, summing up the effect of each chamber,

$$C_{D_S} = \Sigma\, (Q_a \Delta p_a)/(q_\infty S U_\infty)$$

with $\Delta p_a = p_\infty + q_\infty - p_a$ where p_a is the internal static pressure and subscript a designates a particular chamber. Defining C_{Q_a} as Q_a/SU_∞ and C_{p_a} as $p_a - p_\infty/q_\infty$, the suction drag coefficient reduces to

$$C_{D_S} = \Sigma\, C_{Q_a}(1 - C_{p_a})$$

The equivalent drag coefficient due to shell-pressure drop is

$$C_{D_{SS}} = \Sigma\, Q_a(p_a - p_e)/(q_\infty U_\infty S) = -\Sigma\, C_{Q_a}(C_{p_a} - C_{p_e})$$

where p_e is the static pressure outside the shell. Further details on data reduction and accuracy can be obtained from Ref. 7.

Looking at the modified data in Fig. 6 and 7, it is seen that for optimum C_Q, $C_{D_{SM}}$ is approximately half C_{D_W}, and that $C_{D_{SM}}$ increases linearly with C_Q. Also, it is seen that C_{D_W} reduces with increasing C_Q up to about 2.1×10^{-4}, beyond which it stays approximately constant or increases. A significant increase in C_{D_W} takes place for $R_l > 11 \times 10^6$ because the boundary layer becomes turbulent due to wind-tunnel turbulence and vibration.

Since the ideal static-pressure coefficient across the shell, $C_{p_a} - C_{p_e}$, is approximately -0.10, the ideal value of

$$C_{D_{SS}}/C_{D_S} = -(C_{p_a} - C_{p_e})/1 - C_{p_a}$$

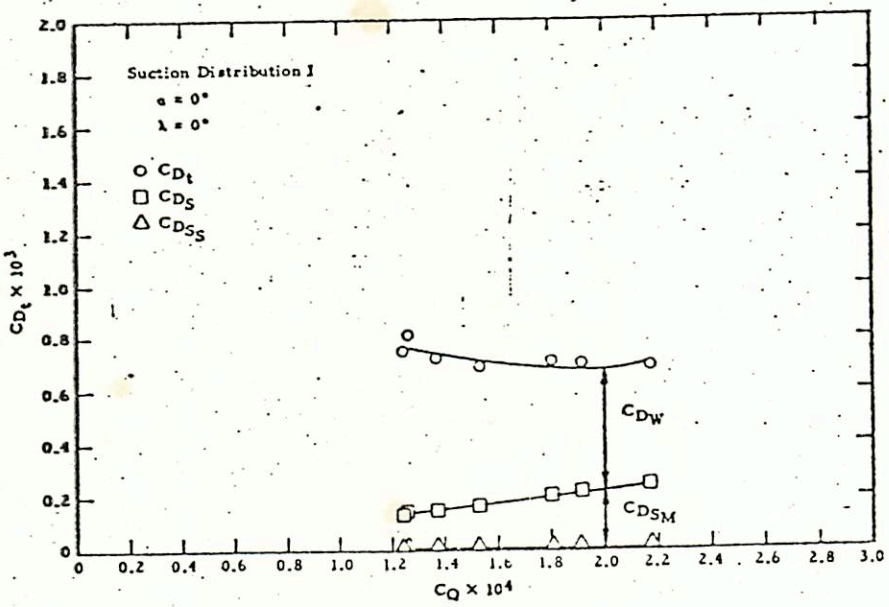

FIG. 6. Components of Modified Drag as a Function of Suction Rate; $R_\ell = 8 \times 10^6$.

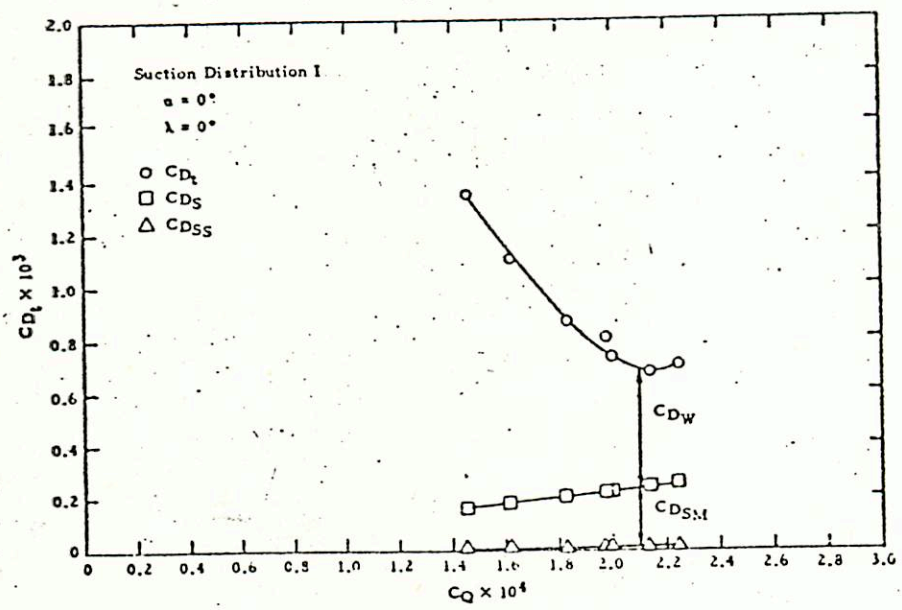

FIG. 7. Components of Modified Drag as a Function of Suction Rate; $R_\ell = 11 \times 10^6$.

is less than 0.10. It may be inferred that in a prototype torpedo configuration, where $C_{D_S} \approx C_{D_W}$, the drag due to shell-pressure drop is around 5% of the total drag.

RELATIVE MAGNITUDE OF DRAG COMPONENTS

Figures 6 - 9 show the components of total drag as a function of suction rate for both the original data and the modified data for $R_\ell = 8$ and 11×10^6. These figures show that the drag arising from shell permeability is approximately 1/4 the total drag before modification, but is extremely low after modification. Thus the total drag is reduced by approximately 25% when modified for shell permeability.

EFFECT OF ROUGHNESS

At the lower Reynolds numbers of Fig. 6 and 9, there is no significant change in C_{D_W} with higher values of C_Q, indicating that there is probably no problem with roughness, at least in this range. Increasing C_Q, it should be noted, reduces the thickness of the boundary layer, which makes roughness more critical and also increases the wall shear stress. This result would indicate that when the wind-tunnel conditions are nonturbulent and vibration-free, there is no sign of adverse model roughness. This lack of roughness indicates that the same model could be tested at a higher Reynolds number in a wind tunnel with lower turbulence and vibration, and still maintain a laminar boundary layer.

EFFECT OF LONGITUDINAL MODEL SEAMS

Figure 10 shows how wake drag varied appreciably around the body, and how this variation depended on suction rate. Rakes 1, 4, and 6, located along Seams 1, 3, and 4, are compared with each other and with Rake 5 midway between Seams 3 and 4. To make this comparison, C_{D_W} was calculated singly from each rake. It is seen that Seam 3 is unusually good, Seam 4 unusually bad, Seam 1 bad at lower C_Q and average at high C_Q, assuming that a typical body segment (Rake 5) has average characteristics. Part of this behavior could be explained if large upflow existed on the model at $\alpha = 0°$. It is believed, however, that a more feasible explanation is that the region around Seam 4 is nearly impermeable, that Seam 3 is more permeable than average, and that Seam 1 exhibits characteristics of roughness. This viewpoint is in part supported by the data in Fig. 4 showing that the drag of Seam 4 declined when the model was placed at an angle of attack, α, of 3° to 4°, indicating that inadequate suction existed along the seam at $\alpha = 0°$.

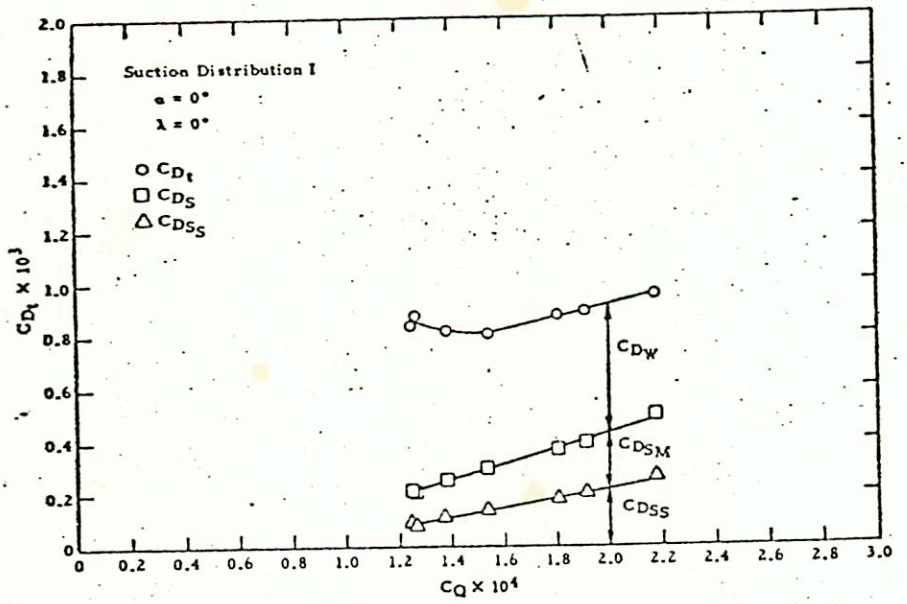

FIG. 8. Components of Drag as a Function of Suction Rate; $R_\ell = 8 \times 10^6$.

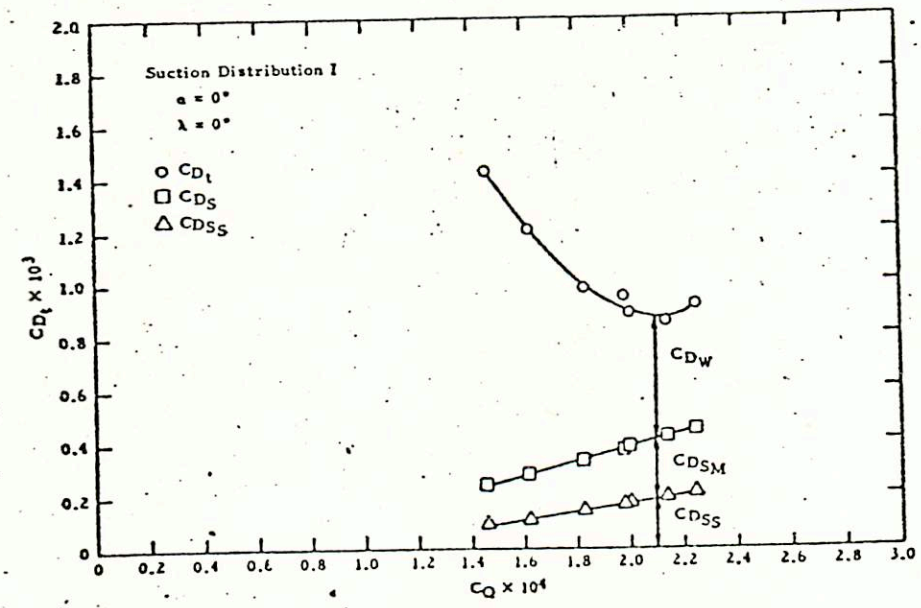

FIG. 9. Components of Drag as a Function of Suction Rate; $R_\ell = 11 \times 10^6$.

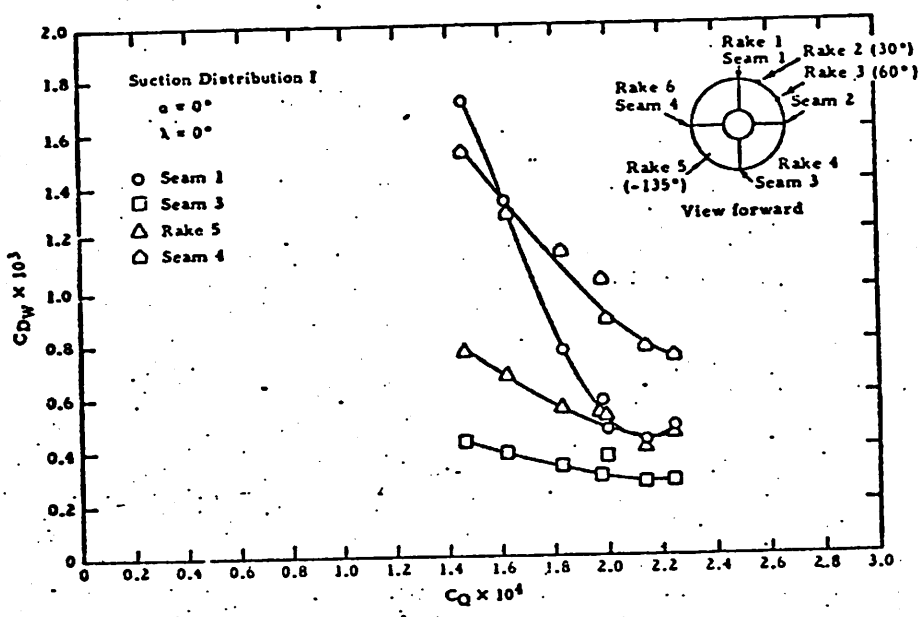

FIG. 10. Effect of Suction Rate on Wake Drag at Various Rake Positions.

BOUNDARY-LAYER PROFILES

EFFECT OF INCREASED SUCTION

An interesting sequence of boundary-layer profiles is shown in Fig. 11 - 17, for Rakes 1 - 6, with $R_\ell = 11 \times 10^6$ and $C_Q = 1.46$ to 2.25×10^{-4}. Of general interest is the fact that the profiles vary considerably around the body, as was implied by Fig. 10. At the lowest suction rate, it is seen that the profiles at Rakes 1, 2, 3, and 6 are generally turbulent, that the profile at Rake 5 is transitional, and that the profile at Rake 4 is essentially laminar. As the suction rate increases, two effects are seen. One is that the boundary layer at Rake 3 goes from essentially turbulent flow to an almost-separated laminar flow (as in an adverse pressure gradient), whereas the boundary layers of the other rakes (except Rake 6) tend to become more laminar, particularly above $C_Q = 1.8 \times 10^{-4}$. Rake 6 (Seam 4) remains essentially turbulent throughout the whole suction range; this is probably due to this seam being less permeable than the rest of the shell. As previously stated, Seam 3 (Rake 4) appears to be more permeable than any other part of the shell because its profile becomes laminar at such low values of C_Q. The separation tendency of Rake 3 (which is located between seams) is undoubtedly due in part to the adverse pressure gradient at the rakes caused by the rake-support ring. It is believed that with increased suction, the tendency to separate would be

eliminated. In Fig. 17, Rakes 1 and 2 show a slight tendency toward separation, in contrast to Rakes 4 and 5, indicating the presence of a slight upflow about the rear of the model, even though $\alpha = 0°$. In a prototype configuration, therefore, it may be desirable to design for an increased suction rate in regions where an adverse pressure gradient might exist, since the resulting pressure drag could be significantly high.

EFFECT OF REYNOLDS NUMBER

The effect of the Reynolds number on the boundary-layer profile is shown in Fig. 18 and 19 for Rakes 5 and 3, respectively, with $C_Q = 2 \times 10^{-4}$. It is seen that the boundary layer for Rake 5 is becoming turbulent as R_ℓ approaches 11.5 to 12×10^6, owing to tunnel turbulence and vibration. The boundary layer is essentially laminar up to that point and becomes thinner as the Reynolds number increases. The boundary layer at Rake 3, however, is very different under identical conditions. As previously stated, this tendency toward separation is attributed to the effect of a greater adverse pressure gradient and possibly to a region of reduced permeability. Note, however, that this tendency to separate becomes less marked as the Reynolds number increases. This is to be expected, since the boundary layer is becoming thinner.

PROFILES WITH NO SUCTION

Figure 20 shows the turbulent boundary layers at Rakes 1 - 6 for $R_\ell = 11 \times 10^6$ and no suction. The variations between rakes are probably due to differences in shell roughness and rake calibration. For example, Rake 4 appears to produce 19% higher drag than Rake 5.

EFFECT OF ANGLE OF ATTACK

The effect of attack angle on boundary-layer profile is shown in Fig. 21 - 24, where $R_\ell = 11 \times 10^6$, $C_Q = 2 \times 10^{-4}$ and $\alpha = 0$, 2, 3, and 4°. Several conclusions can be drawn from these figures. Looking at the profiles for Rakes 4 and 5, located near the bottom of the model, it is seen that the effect of increasing α is to reduce the laminar-profile thickness. This behavior is to be expected because the crossflow thins the boundary layer and the pressure gradient becomes more favorable on the lower side as α increases. The effect of α at Seam 4 (Rake 6) shows that the boundary layer is primarily turbulent at $\alpha = 0$ and 2°, while at $\alpha = 3°$ it is predominantly laminar, and then is less laminar at $\alpha = 4°$. This result would be predicted if Seam 4 were somewhat impermeable; the transitional behavior at the side of a body in high crossflow is normal. Rake 1 is located at Seam 1 at the top of the model and appears to remain laminar throughout the range of varying

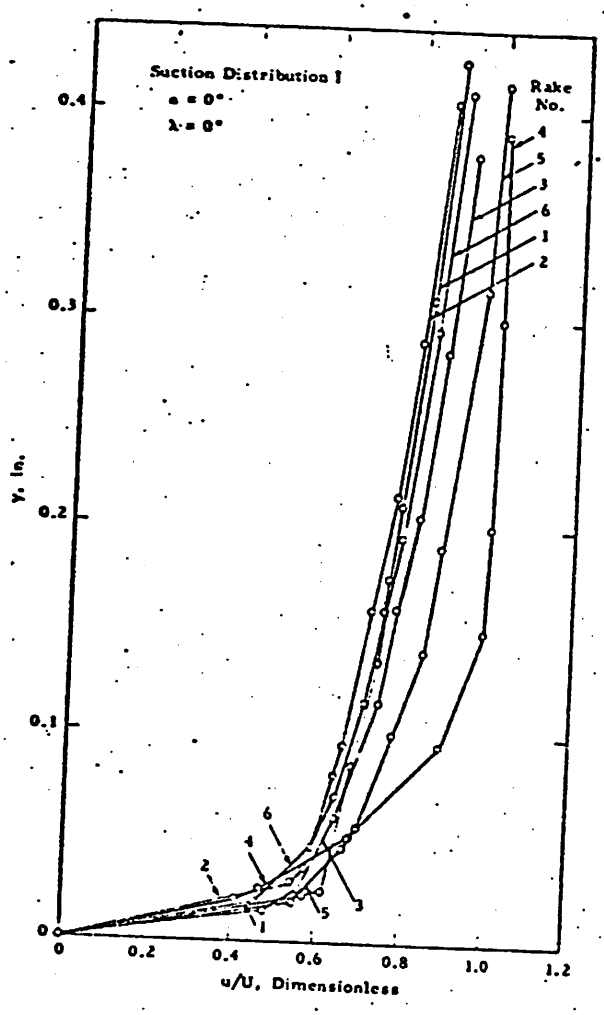

FIG. 11. Boundary-Layer Profiles; $R_\ell = 11 \times 10^6$, $C_Q = 1.46 \times 10^{-4}$.

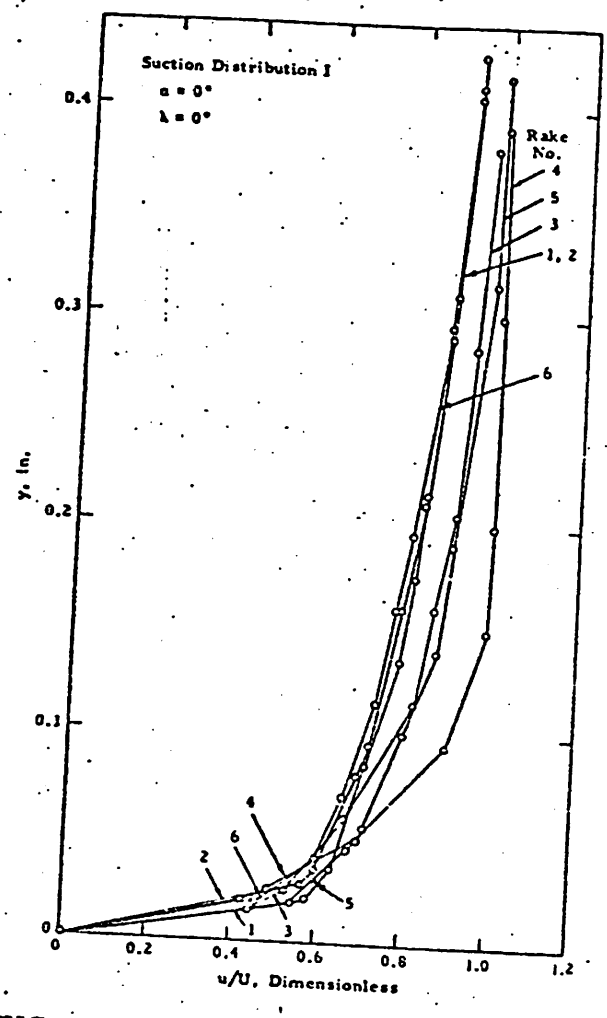

FIG. 12. Boundary-Layer Profiles; $R_\ell = 11 \times 10^6$, $C_Q = 1.62 \times 10^{-4}$.

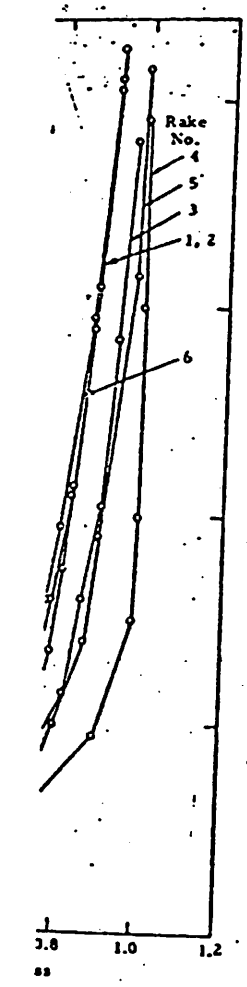

Profiles;
$\times 10^{-4}$.

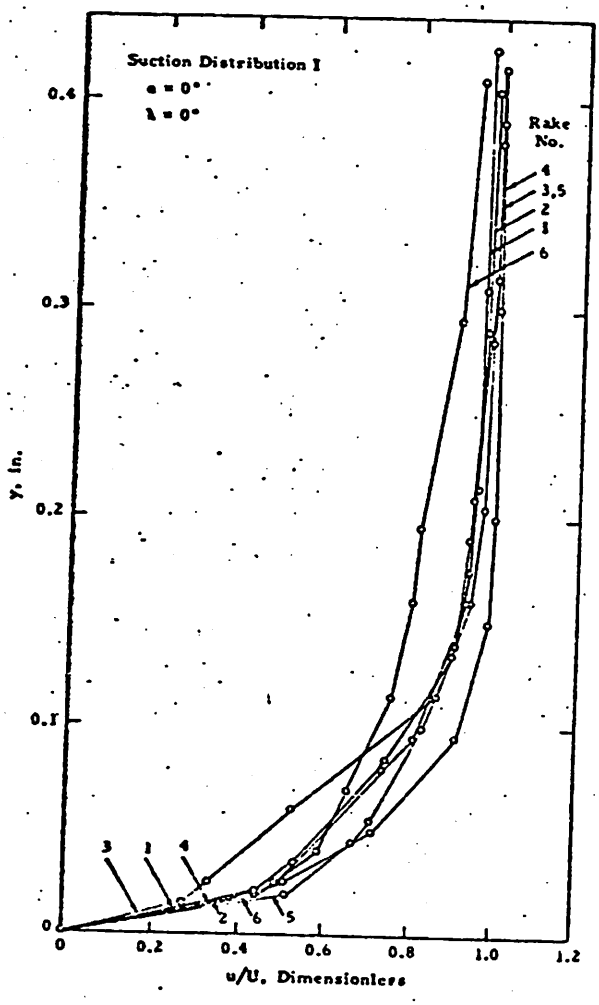

FIG. 13. Boundary-Layer Profiles; $R_\ell = 11 \times 10^6$, $C_Q = 1.83 \times 10^{-4}$.

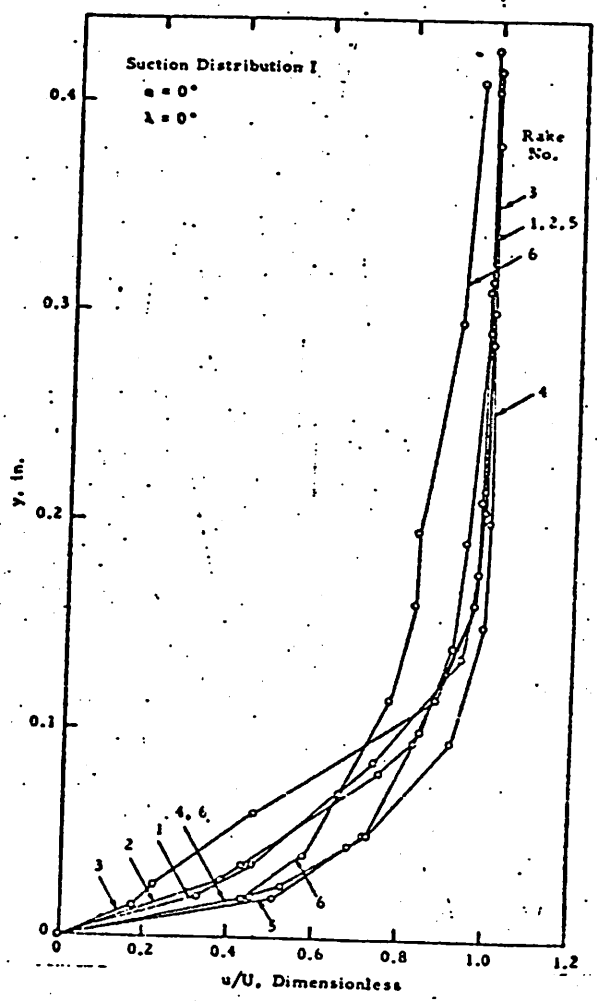

FIG. 14. Boundary-Layer Profiles; $R_\ell = 11 \times 10^6$, $C_Q = 1.98 \times 10^{-4}$.

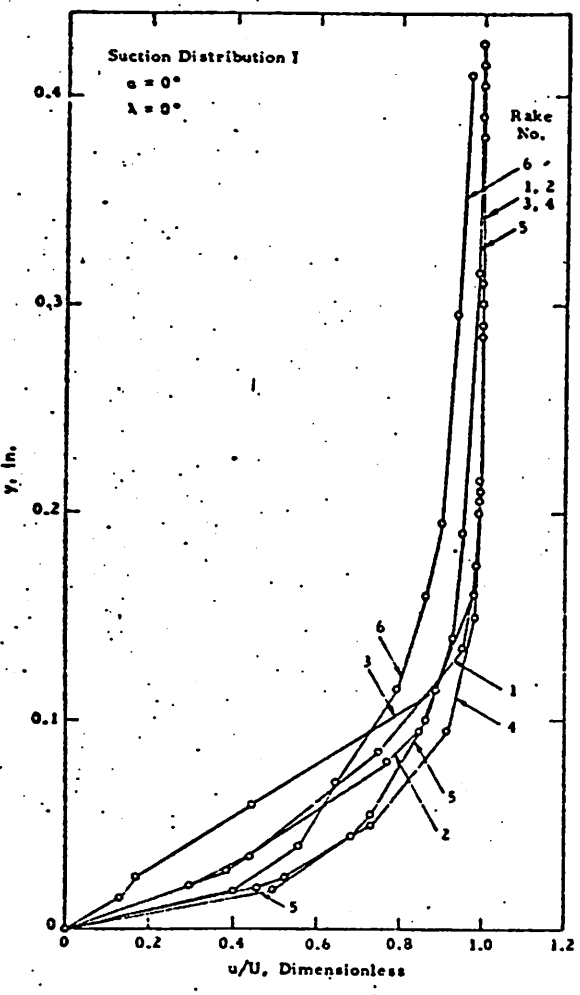

FIG. 15. Boundary-Layer Profiles; $R_\ell = 11 \times 10^6$, $C_Q = 2.00 \times 10^{-4}$.

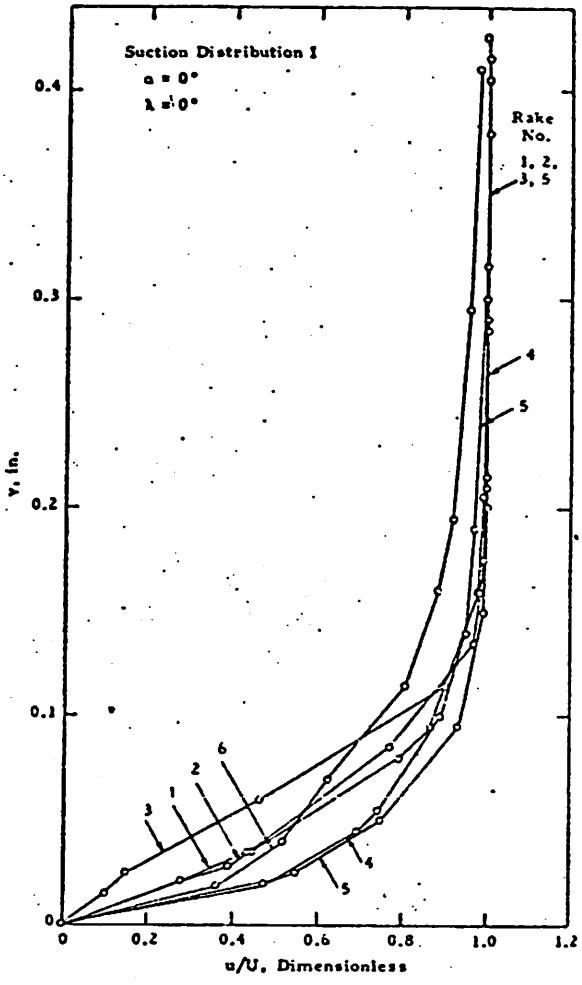

FIG. 16. Boundary-Layer Profiles; $R_\ell = 11 \times 10^6$, $C_Q = 2.14 \times 10^{-4}$.

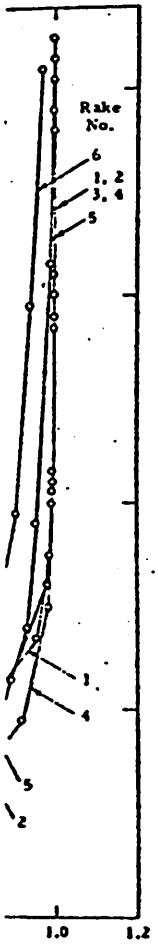

rofiles;
10^{-4}.

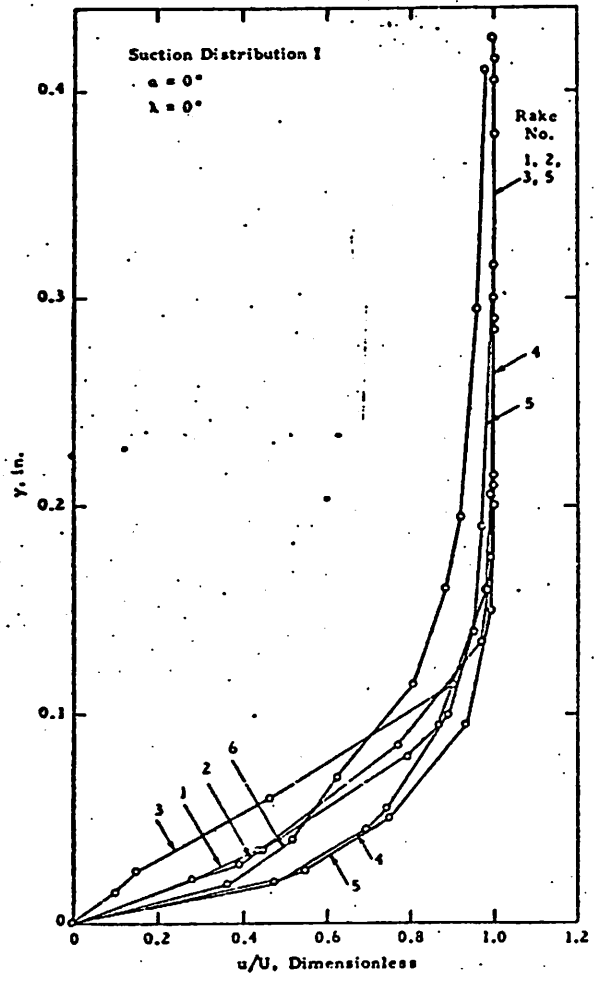

FIG. 16. Boundary-Layer Profiles; $R_\ell = 11 \times 10^6$, $C_Q = 2.14 \times 10^{-4}$.

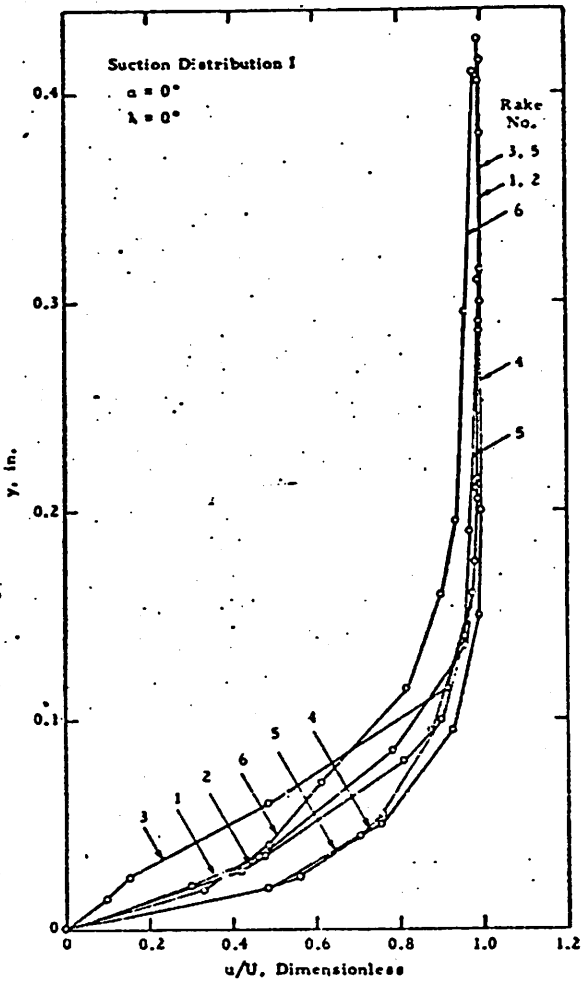

FIG. 17. Boundary-Layer Profiles; $R_\ell = 11 \times 10^6$, $C_Q = 2.25 \times 10^{-4}$.

2

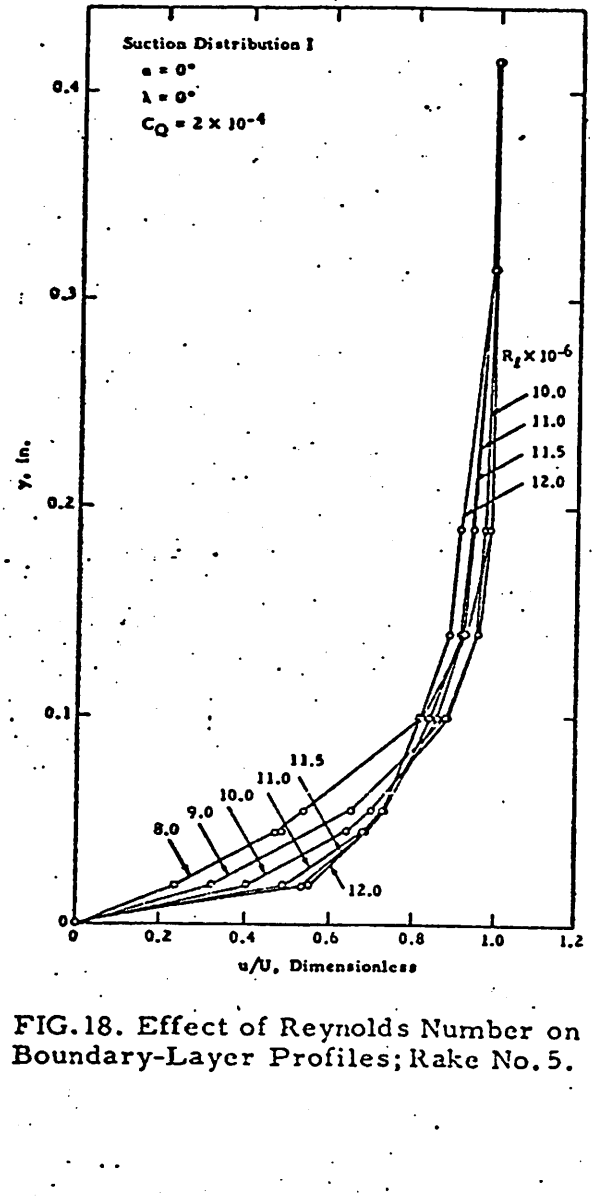

FIG. 18. Effect of Reynolds Number on Boundary-Layer Profiles; Rake No. 5.

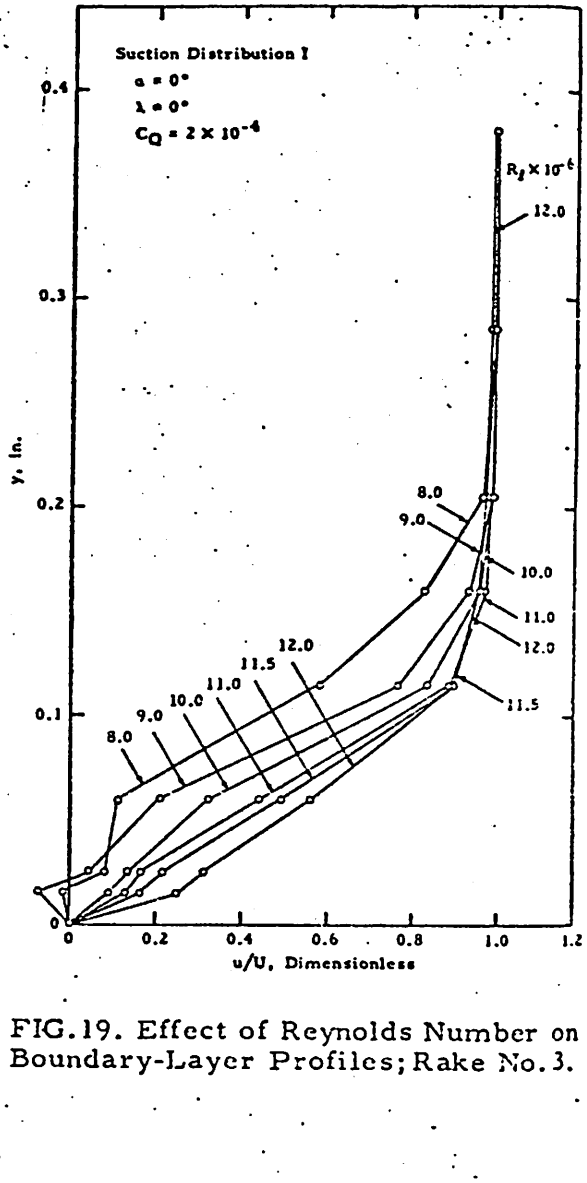

FIG. 19. Effect of Reynolds Number on Boundary-Layer Profiles; Rake No. 3.

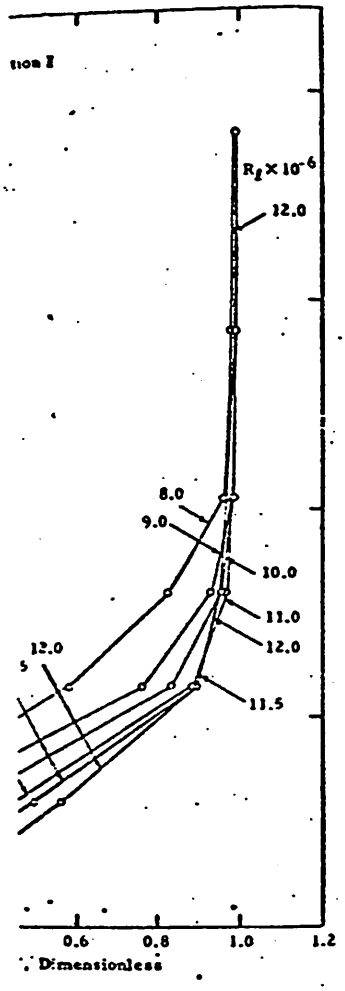

Reynolds Number on Profiles; Rake No. 3.

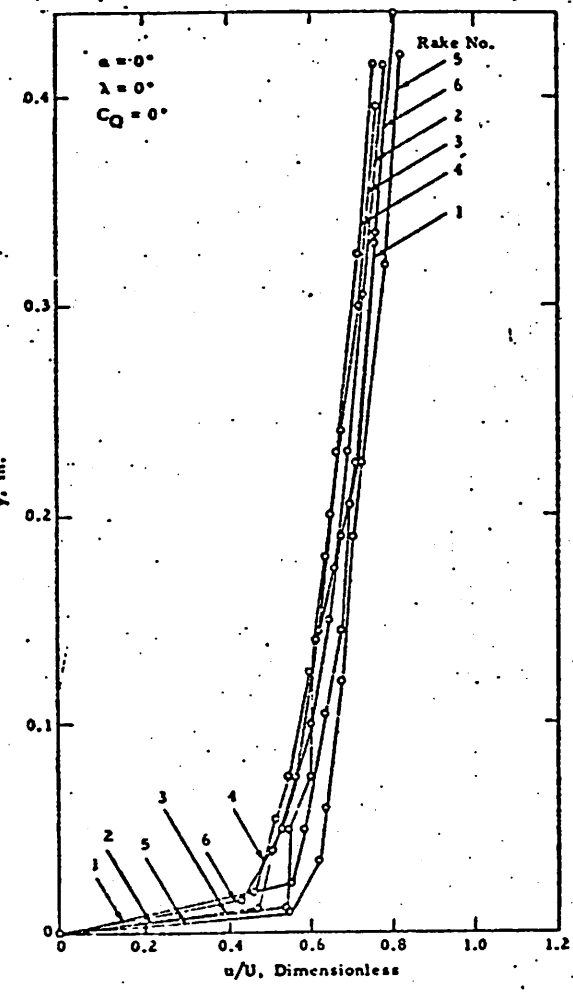

FIG. 20. Boundary-Layer Profiles With No Suction; $R_l = 11 \times 10^6$.

2

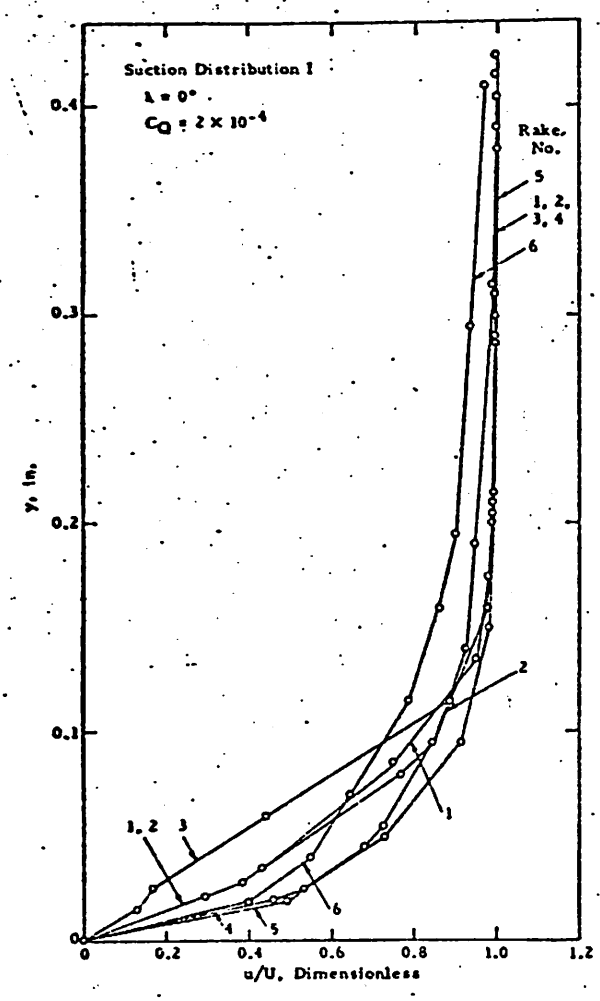

FIG. 21. Boundary-Layer Profiles; R_ℓ = 11 × 10⁶, α = 0 deg.

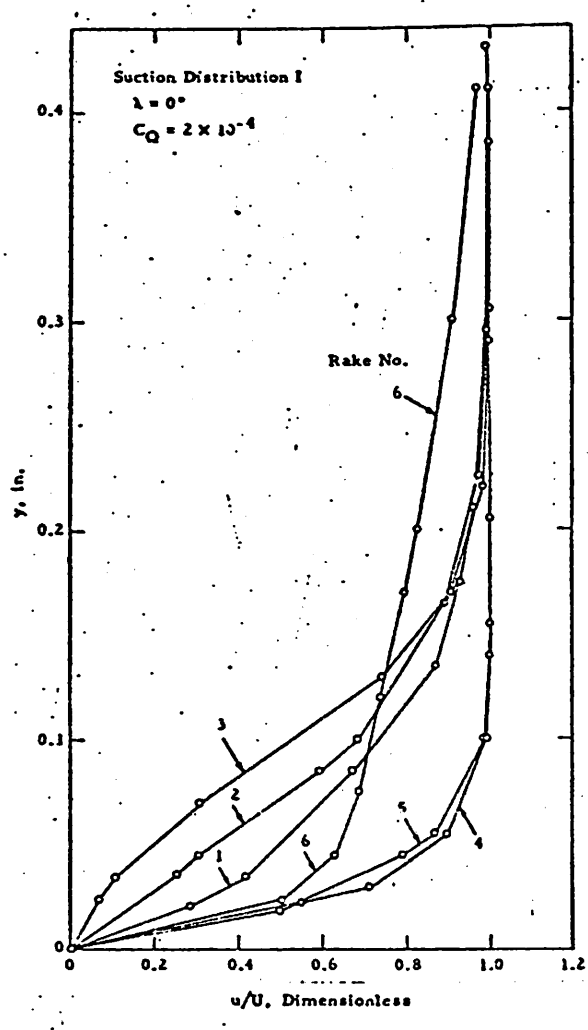

FIG. 22. Boundary-Layer Profiles; R_ℓ = 11 × 10⁶, α = 2 deg.

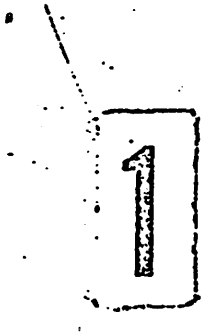

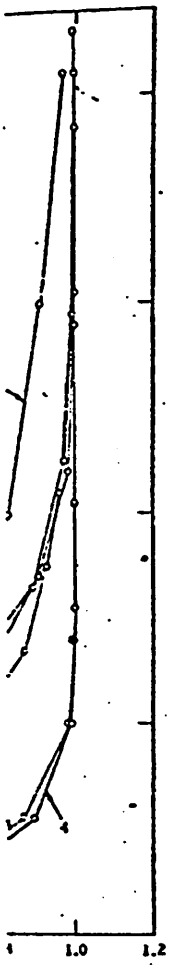

Profiles;

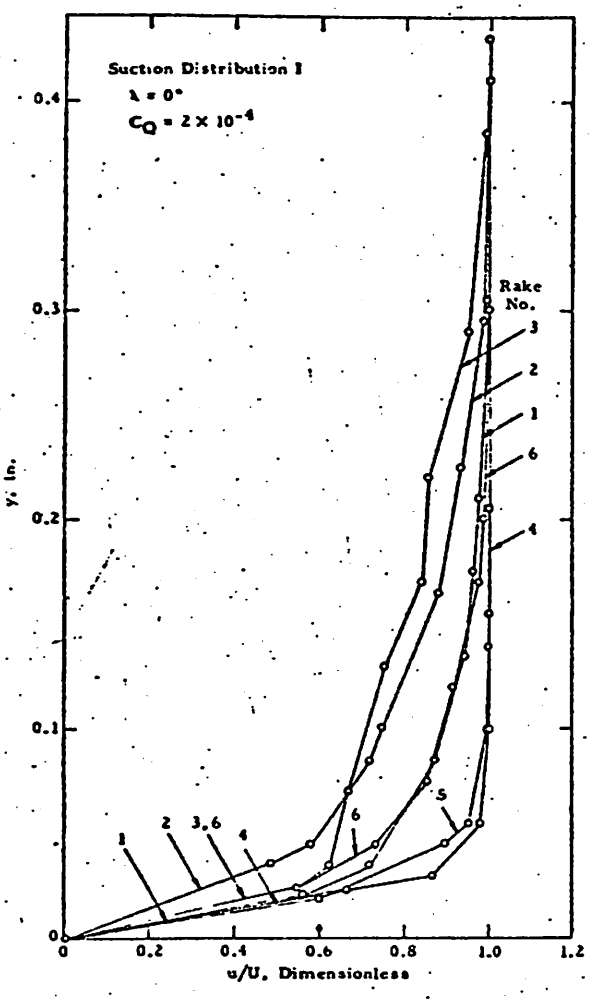

FIG. 23. Boundary Layer Profiles; $R_\ell = 11 \times 10^6$, $\alpha = 3$ deg.

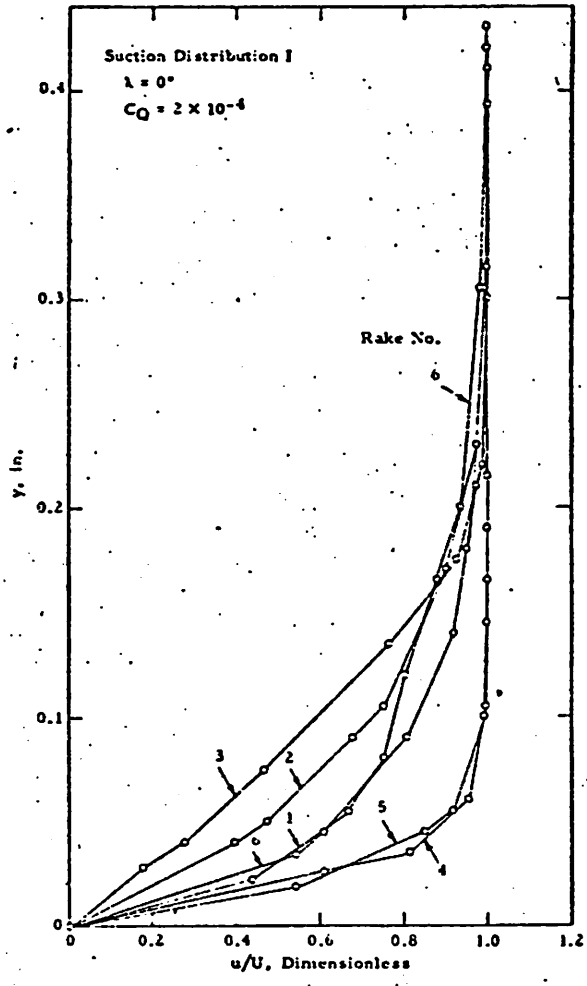

FIG. 24. Boundary-Layer Profiles; $R_\ell = 11 \times 10^6$, $\alpha = 4$ deg.

angle of attack. Rake 3, however, exhibits a tendency toward separation at $\alpha = 0°$ and 2°, toward turbulence at $\alpha = 3°$, and then a tendency toward separation again at $\alpha = 4°$. Rake 2, on the other hand, shows a slight tendency toward separation at $\alpha = 0°$, a greater tendency at $\alpha = 2°$, and then a state that is almost separated, lying between turbulent and laminar flow at $\alpha = 3°$ and 4°.

DATA VARIATIONS BETWEEN RAKES

The effect of suction rate on boundary-layer profiles is shown in Fig. 25 - 27 for Rakes 2, 3, and 5, respectively, at $\alpha = 0°$ and $R_\ell = 11 \times 10^6$. Even though conditions are identical, the results from these three rakes are quite different. Looking first at Rake 2, it is seen that the boundary layer is partially turbulent up to a suction coefficient of 2×10^{-4} and is essentially laminar above this point, becoming thinner as suction is increased. There is no sign of increased wake drag as suction increases, indicating that roughness is not a problem at this particular body station and Reynolds number. The profiles at Rake 3 indicate that the boundary layer is essentially turbulent for C_Q up to 1.91×10^{-4}, and that it is laminar with a tendency toward separation above 2×10^{-4}. The results from Rake 5 show turbulence up to C_Q of 2.16×10^{-4}, and full laminar flow above 2.3×10^{-4}.

EFFECT OF SUCTION DISTRIBUTION

Figures 28 and 29 show the effect of suction distribution on the boundary layer for Rakes 2 and 5, respectively, for $R_\ell = 9 \times 10^6$, $C_Q = 1.5 \times 10^{-4}$, and $\alpha = 0°$. In general, the results indicate that the boundary layer is partially turbulent for Suction Distributions I and III, with a tendency toward laminar flow (Rake 5) and separation (Rake 2) for Suction Distribution II.

EFFECT OF 45° MODEL ROTATION WITH RAKES REMAINING FIXED IN SPACE

The wake drag is shown in Fig. 30 as a function of rake number both in the normal model position and with the model shell rotated 45° clockwise, looking forward. Thus the portion of the shell measured normally by Rake 5 is now being measured by Rake 6, and Seam 3, normally measured by Rake 4, is now being recorded by Rake 5. Looking at the data from these two locations, it appears that the readings taken by Rakes 4 and 5 of Seam 3 are essentially in agreement, and that the reading of the shell at -135° is different by about 25%, as measured by Rakes 5 and 6. This difference is due either to errors in rake calibration or to suspected upflow in the wind tunnel. The faultiness of Seam 4 is readily apparent, since before rotation Rake 6 measured

a wake-drag coefficient of 0.88×10^{-3}, which is approximately twice as high as the average of the other readings. There is a tendency of the wake drag to be higher on the upper side of the body than on the lower side, again indicating a slight upflow. It is apparent that variations in shell characteristics and rake calibration are primary parameters.

PERMEABILITY AND ROUGHNESS OF SEAM 4

Figure 31 shows that as the suction rate increases, the wake drag of Seam 4 continuously decreases; this is a further indication that Seam 4 tends to be impermeable and that there is no apparent problem of roughness.

CONCLUSIONS

The following conclusions may be drawn from this study.

1. The results of the NOTS porous-fiberglass model tests show full laminar flow up to $R_\ell = 12 \times 10^6$, the turbulence and vibration limit of the wind tunnel. Full laminar flow might be obtained at much higher Reynolds numbers, since there is no indication that roughness was a problem, except at Seam 1.

2. The results of the NOTS porous-fiberglass model tests and the Northrop slotted-metal model tests are in general agreement.

3. One longitudinal seam was found to have higher drag, and another lower drag, than other portions of the shell, indicating that seams are not always a problem.

4. A tendency toward laminar separation appeared on the upper side near the rear end of the body where an adverse pressure gradient existed.

5. The total drag coefficient varied little with suction distribution for the range of these tests.

6. Little change in total drag coefficient was noted as a function of α up to 4°, the highest test angle of attack.

7. The permeability of the porous shell did not change significantly with variations in wind speed, Reynolds number, and suction rate.

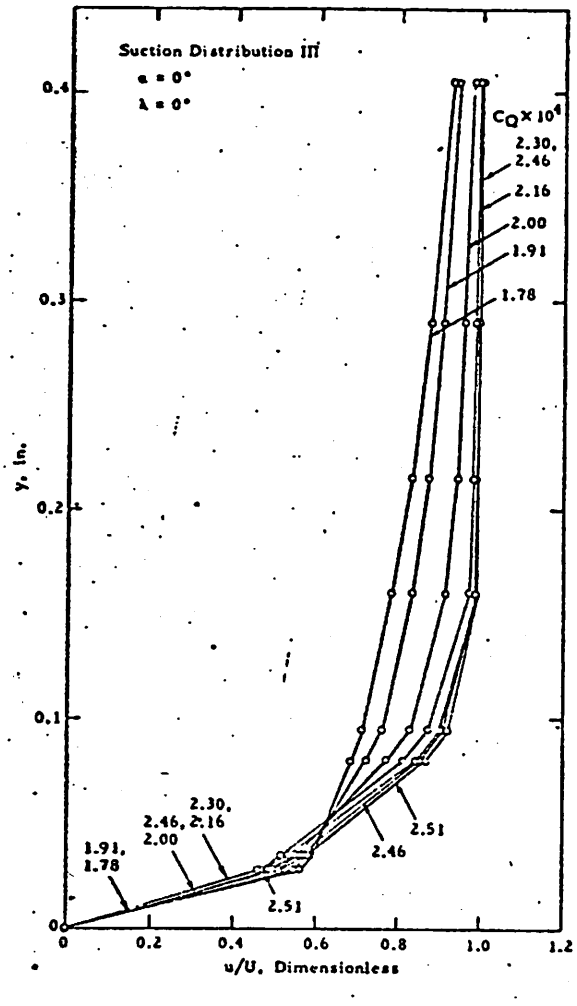

FIG. 25. Effect of Suction Rate on Boundary-Layer Profiles; $R_\ell = 11 \times 10^6$, Rake No. 2.

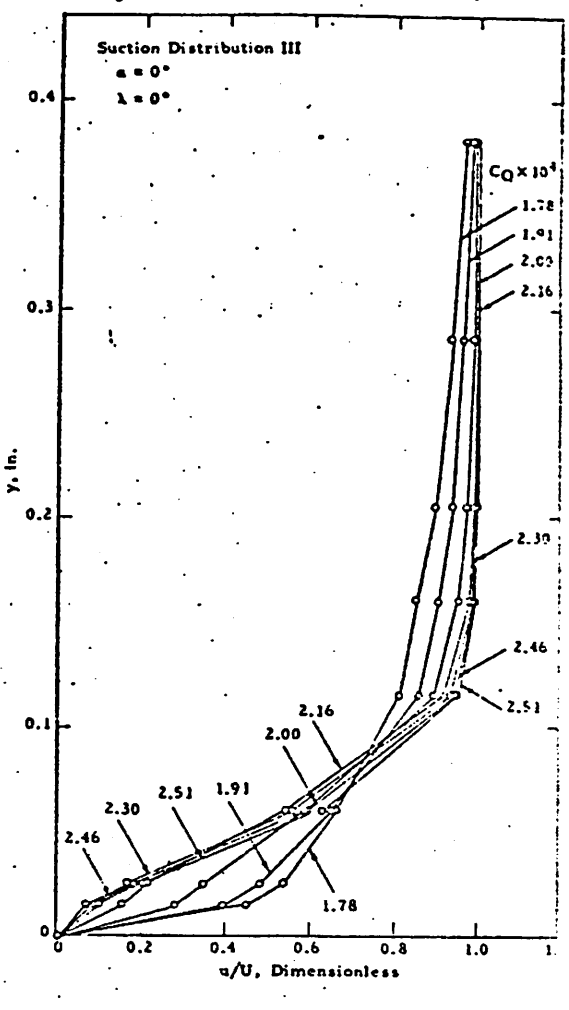

FIG. 26. Effect of Suction Rate on Boundary-Layer Profiles; $R_\ell = 11 \times 10^6$, Rake No. 3.

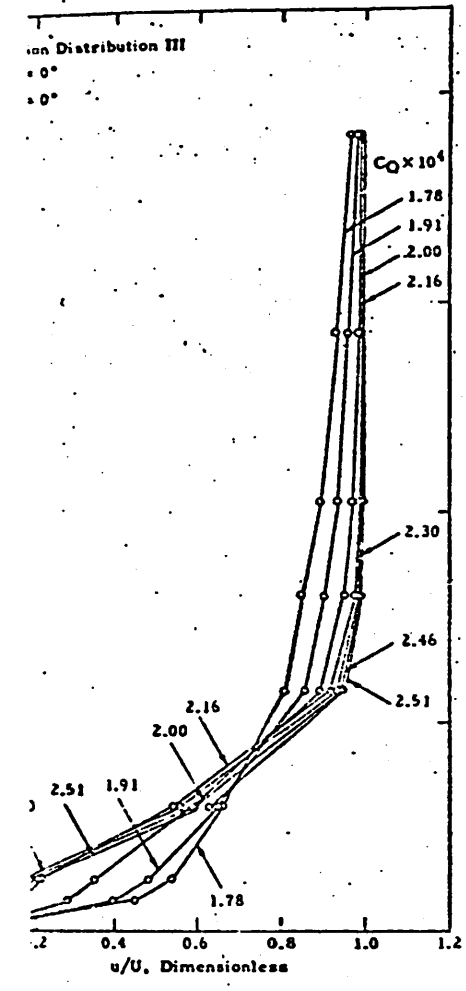

5. Effect of Suction Rate
ndary-Layer Profiles;
$\times 10^6$, Rake No. 3.

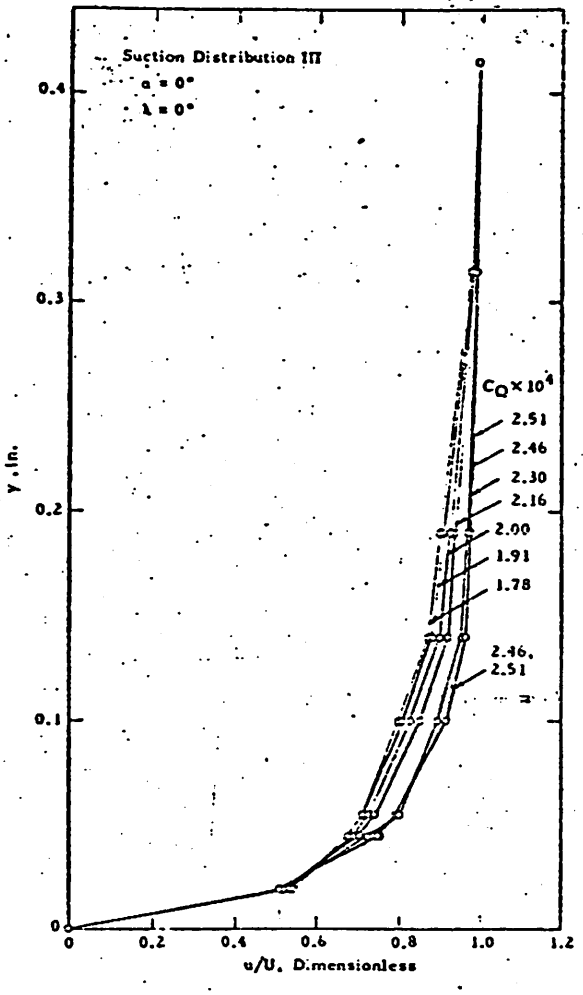

FIG. 27. Effect of Suction Rate on Boundary-Layer Profiles; $R_\ell = 11 \times 10^6$, Rake No. 5.

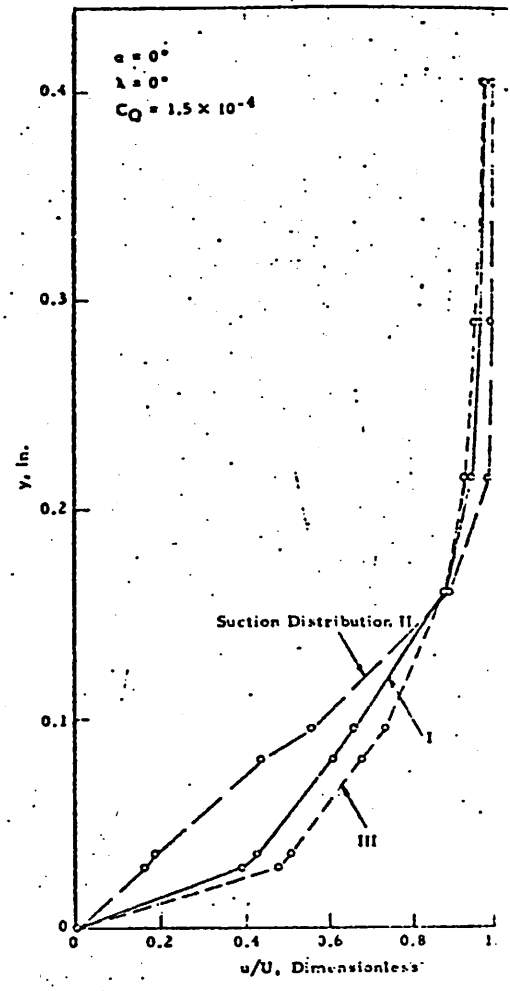

FIG. 28. Effect of Suction Dis
bution on Boundary-Layer Profi
$R_\ell = 9 \times 10^6$, Rake No. 2.

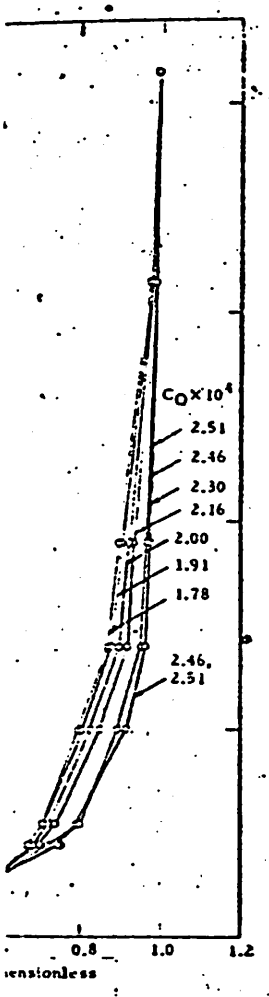

Suction Rate
er Profiles;
ke No. 5.

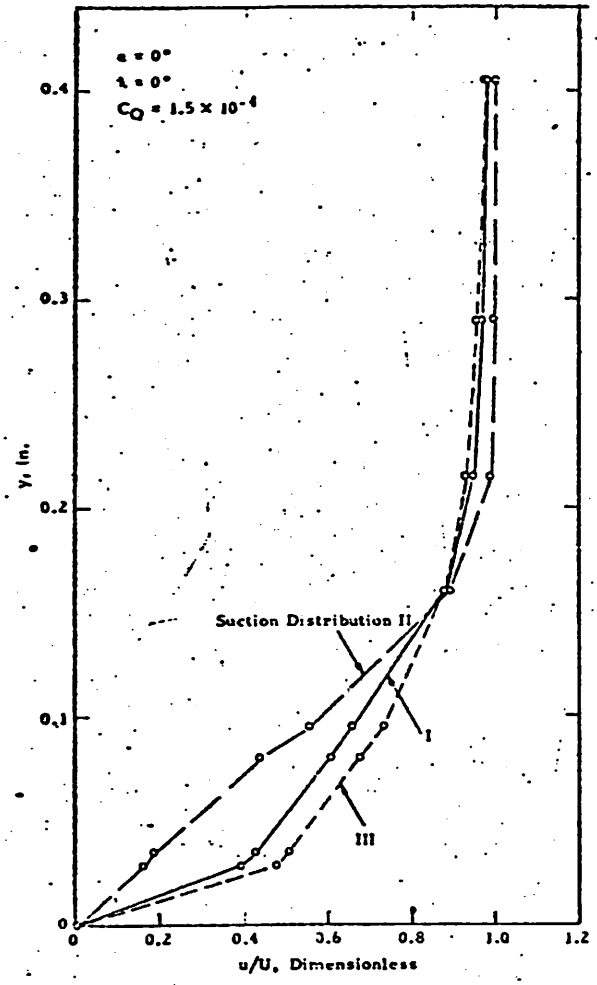

FIG. 28. Effect of Suction Distribution on Boundary-Layer Profiles; $R_\ell = 9 \times 10^6$, Rake No. 2.

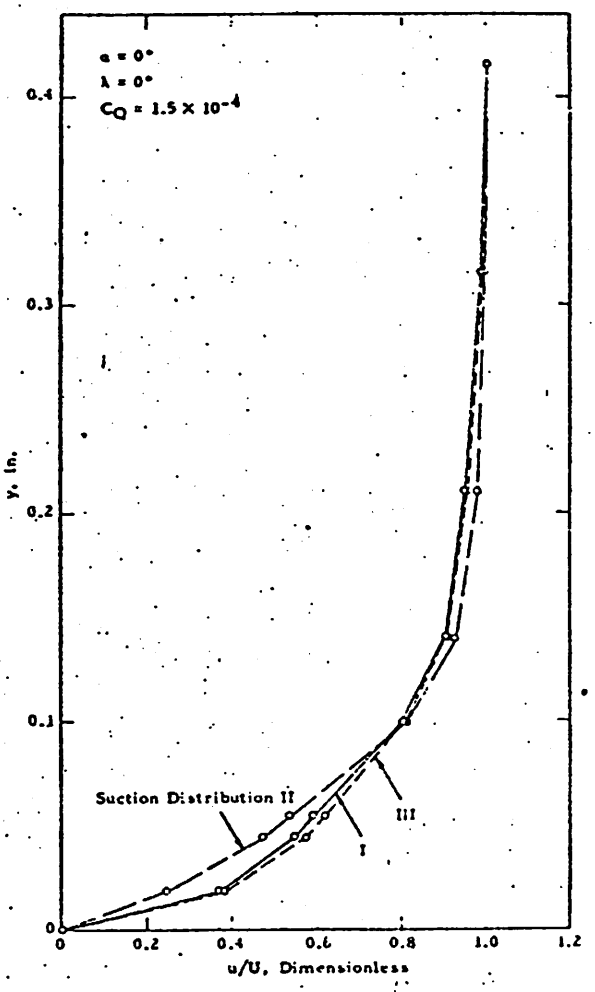

FIG. 29. Effect of Suction Distribution on Boundary-Layer Profiles; $R_\ell = 9 \times 10^6$, Rake No. 5.

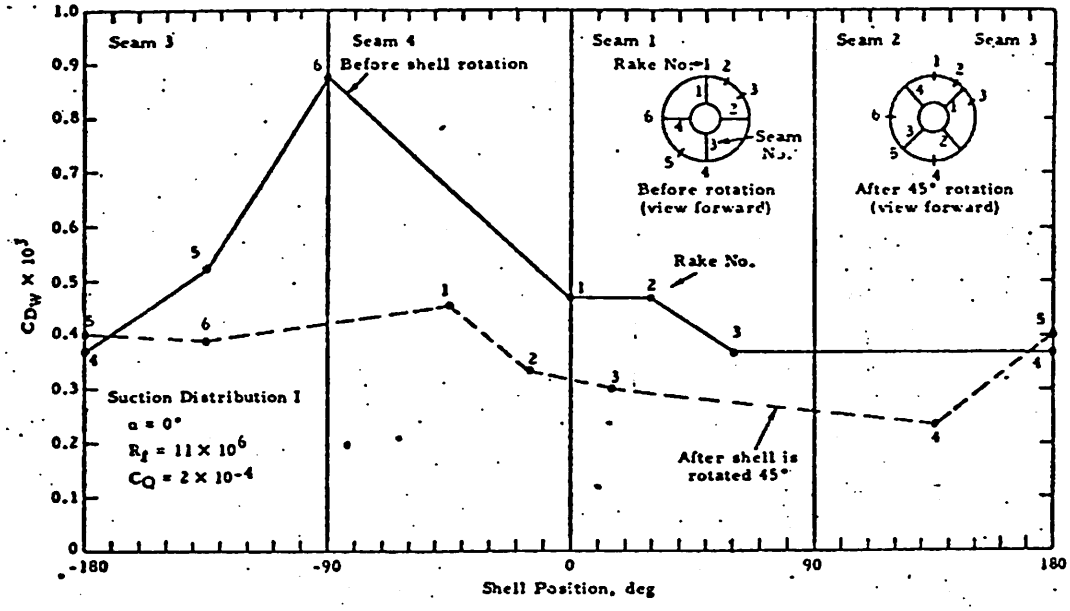

FIG. 30. Wake-Drag Coefficient as a Function of Shell Position.

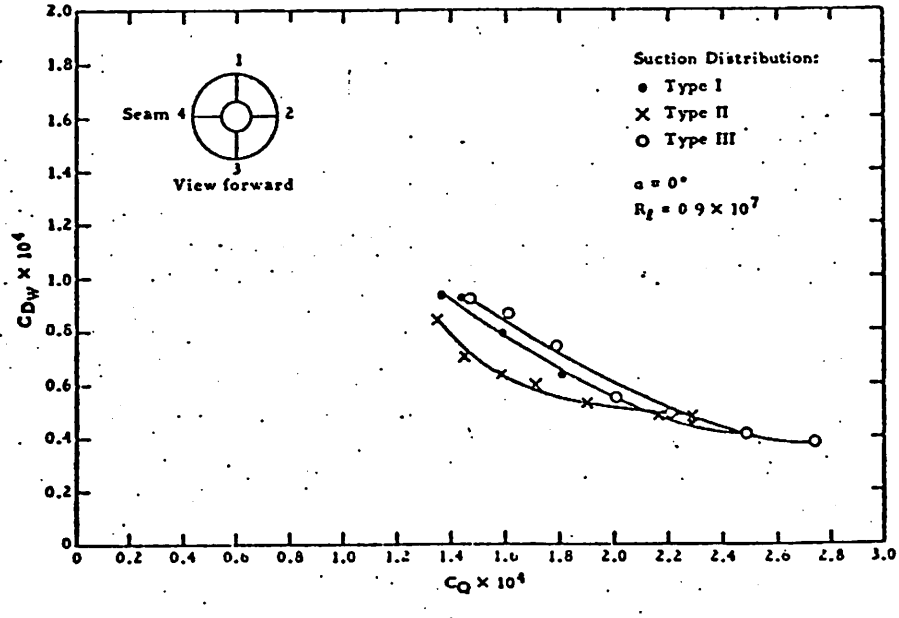

FIG. 31. Effect of Suction Rate on Wake Drag of Seam Four.

Appendix A
MODEL DESCRIPTION

The model selected was an 8:1 modified prolate spheroid 12 3/4 inches in diameter and sting-mounted. The choice of a porous shell was made because area suction is simpler and theoretically more desirable than suction through slots or holes. It was found that such a shell could be fabricated inexpensively, and that clogging need not be a major problem.

It was decided to choose a body of revolution whose shape would produce a predominantly constant pressure distribution for axisymmetric flow. Such a shell produces uniform suction velocity over the area of each suction compartment if permeability is uniform. Fortunately, a body-contour family having the desired characteristics has been identified by Munzner and Reichardt (Ref. 8). On the basis of axial source-sink potential-flow calculations, they concluded that the body family described by the contour y(x), with

$$\left(\frac{x}{a}\right)^2 + \left(\frac{y}{b}\right)^{2.4} = 1, \qquad -a \leq x \leq a$$

should have nearly constant pressure distribution except near the rounded nose and tail. The flow is along the x axis and $b << a$. For the present body, a = 51 inches and b = 6.375 inches. Detailed potential-flow calculations by Douglas Aircraft Corp., using the method of Ref. 9, confirmed the predicted character of this 8:1 Reichardt ovoid's pressure distribution, and the surface-velocity distribution furnished by Douglas has been used in subsequent boundary-layer calculations. Experimental pressure-distribution measurements by Norair agreed with the potential-flow results (Fig. 32).

The shell was made from layers of fiberglass matting placed in a die and compressed from a thickness of about 12 inches to 3/16 inch. Each strand of fiberglass came covered with a microscopic layer of resin, which created a bond at each intersection of the fibers when the resin was cured by heating. The internal structure of the model and two porous-fiberglass half-shells are shown in Fig. 33. The inside of the model[1] is divided into three suction compartments with a line

[1] The design of the internal structure and calculations of stress and shell deflection under suction were conducted by J. D. Bascom and P. F. Reichert of this Station, while J. D. Brooks aided in the early design of the model.

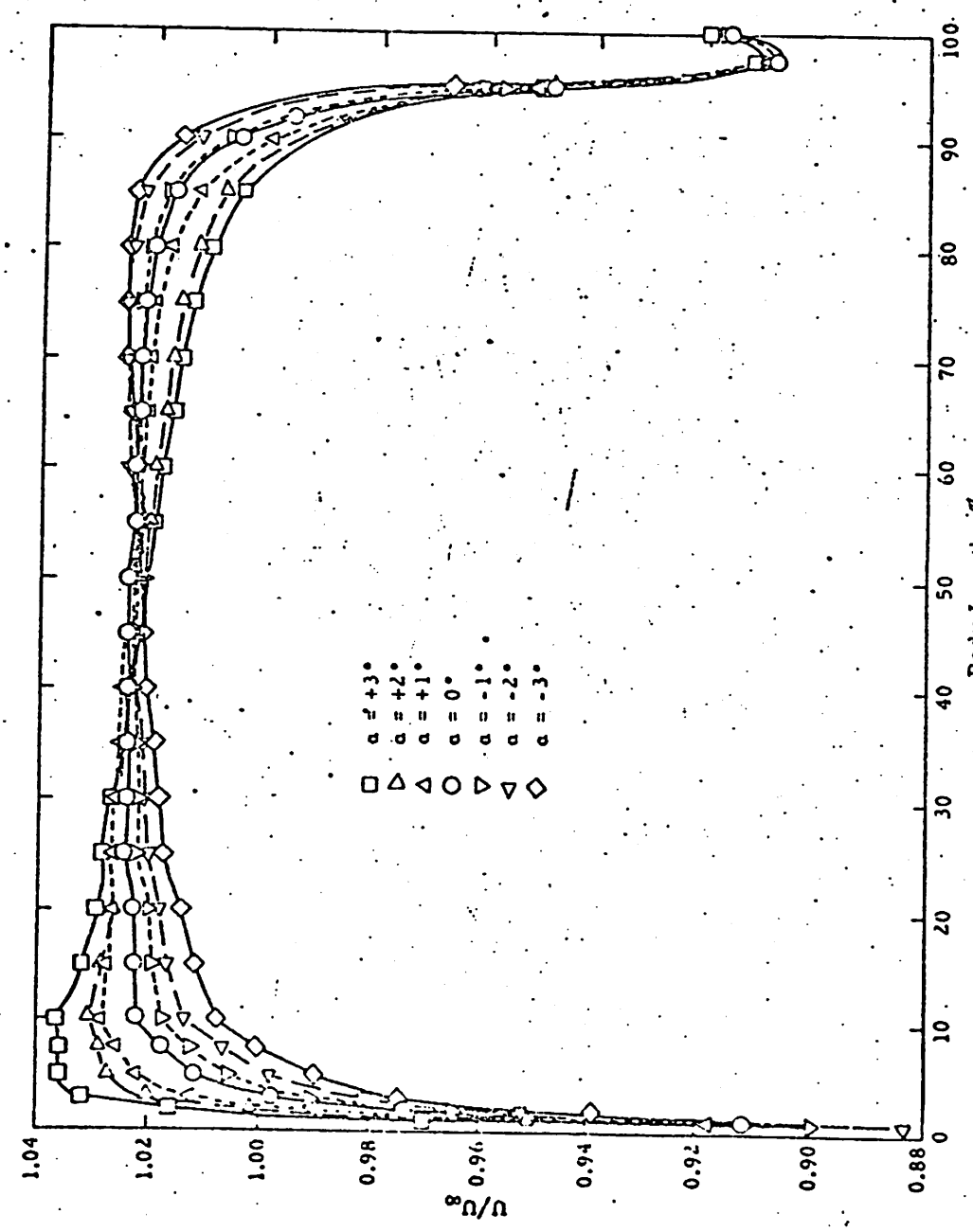

FIG. 32. Velocity Distribution on Northrop's Reichardt Body of Revolution.

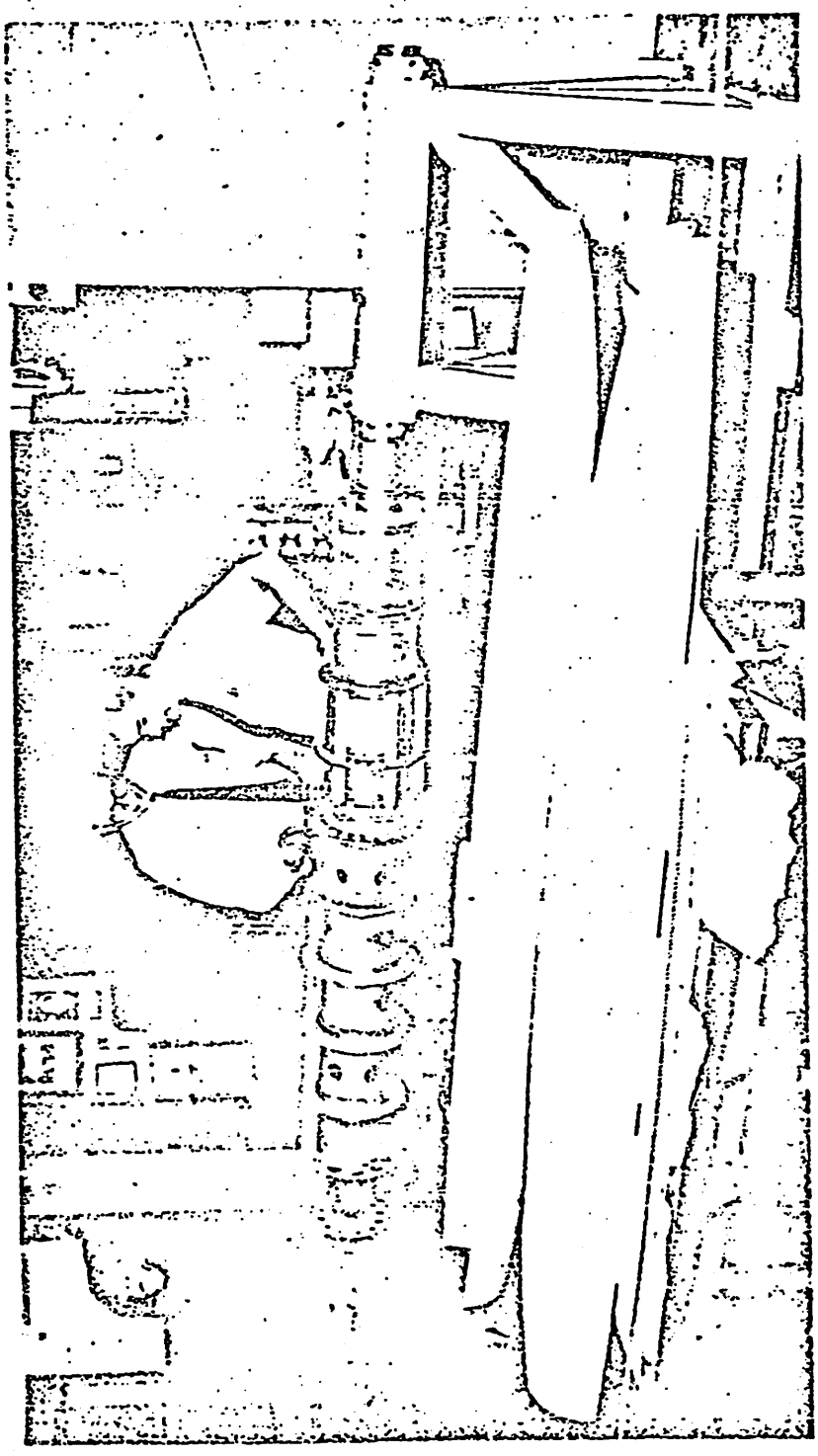

FIG. 33. Internal Structure of the NOTS Porous Model.

leading from each compartment to control valves. Compartment 1 extends from 3 inches to 51 inches behind the nose, Compartment 2 from 51 to 75 inches, and Compartment 3 from 75 to 91 inches.

In Fig. 34 and 35, shell resistivity is presented as a function of soaking time in distilled water. Figure 34 pertains to typical samples from the shell tested at Norair, while Fig. 35 pertains to samples from previously manufactured skins. It is obvious that the resistivity varies radically. The samples become impermeable after four to nine days of immersion, owing to water absorption by the phenolic resin that was used in the manufacturing process. The impermeability arising from long immersion would affect the testing of a model in water, but would not be a factor in the use of a warshot torpedo because of their short running periods. In any case, this problem could be eliminated by the use of waterproof resins.

These changing resistivity characteristics also vary from one set of shells to another, and may vary in magnitude by a factor of two. Such a variance could produce local turbulence if the suction rate is lowered excessively. An example of such a variance is shown in Fig. 36, where the uniform suction pressure of Distribution I produces a non-uniform suction distribution even though all shell segments were made at the same time.

Calculations of allowable roughness height were made, showing that roughness particles of 0.001-inch height at the nose may cause transition on the 45-knot torpedo in water. One such particle will trigger turbulence over a very large percentage of surface area. Extensive experience has been accumulated from aircraft applications (Ref. 6) showing just how critical roughness can be. However, plastic coverings might serve to protect surface finish during handling and launching. These coverings might either be washed or torn away after water contact.

Calculations showed that the direct effect of surface waviness upon boundary-layer stability was unimportant compared to the danger of losing suction over the crests caused by local reduced static pressure.

The primary model specifications include an external tolerance of ±0.015 inch near the nose and tail, and ±0.032 inch at the mid section. Waviness should not exceed 0.001 inch per each half-inch increment, nor 0.01 inch per each 6-inch increment. The mismatch of the nose joint should be less than 0.0005 inch, and the shell thickness should be 0.188 ± 0.01 inch. The shell should be made in eight segments, bonded together with a cement that does not penetrate more than 0.05 inch into the material. The porous-fiberglass tension-yield strength should be at least 2,000 psi, the compression-yield strength 1,400 psi, the tensile modulus of elasticity 225,000 psi, and the compression modulus of elasticity 120,000 psi. Surface roughness should not exceed 15 r.m.s. The model was held within these general specifications.

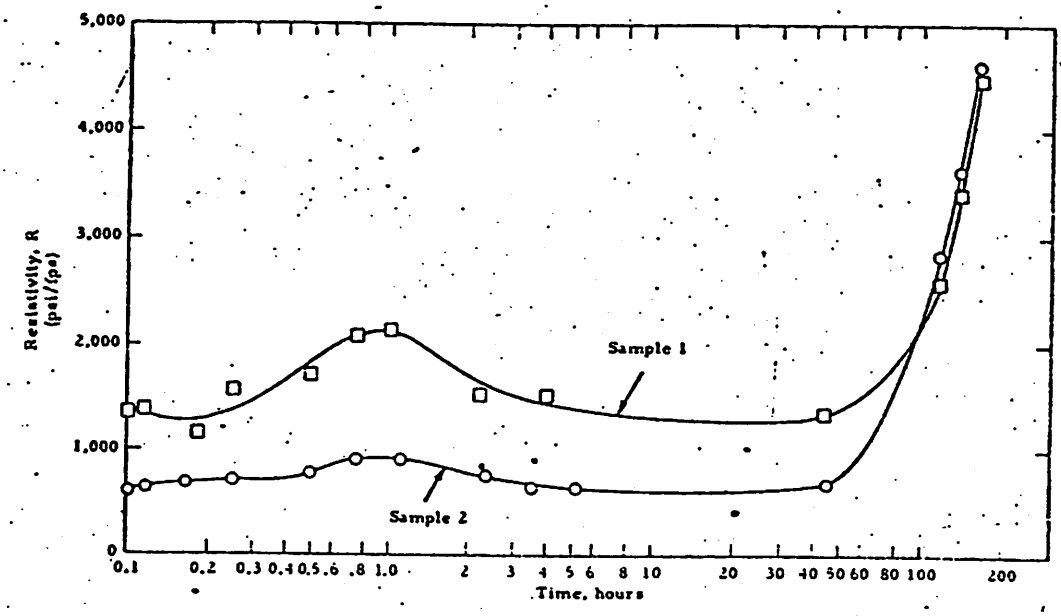

FIG. 34. Shell Resistivity as a Function of Soaking Time in Distilled Water, Samples 1 and 2.

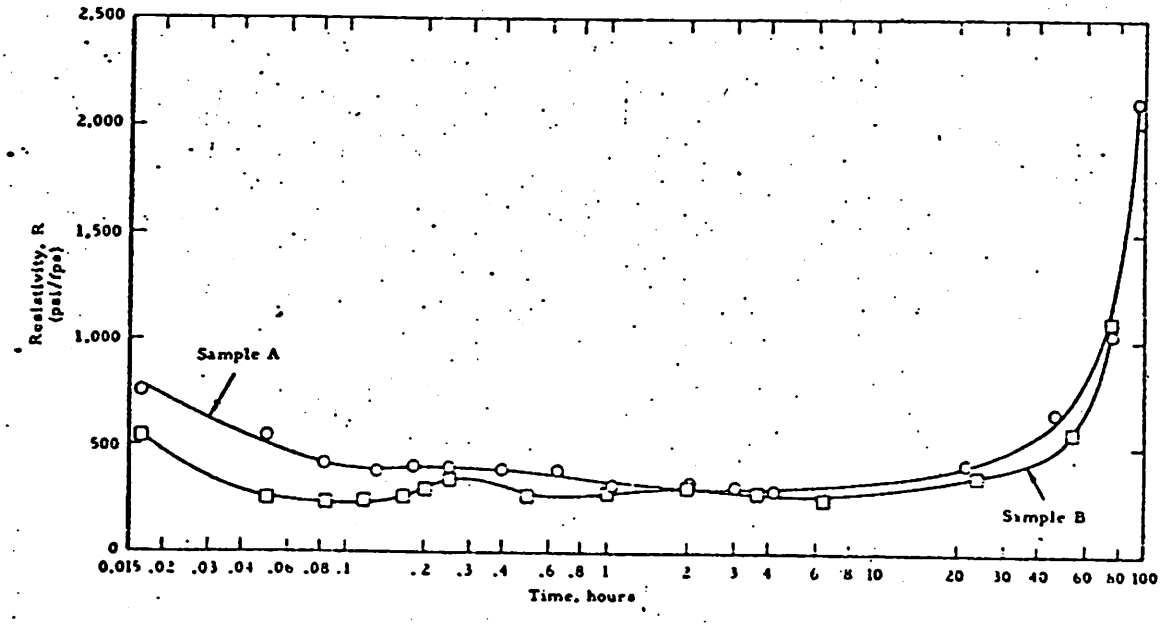

FIG. 35. Shell Resistivity as a Function of Soaking Time in Distilled Water, Samples A and B.

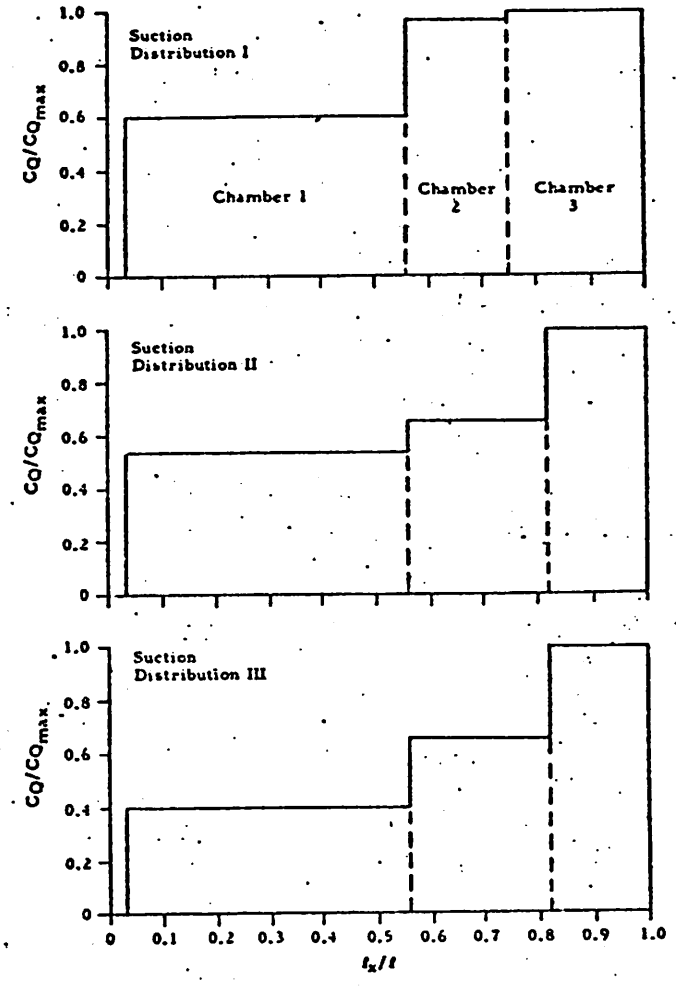

FIG. 36. Relative Suction Distributions.

Northrop provided personnel and instrumentation to check model waviness. Results indicated that most waves were about 6 inches in length, with a maximum trough-to-crest height of about 0.006 inch, and an average trough-to-crest height of about 0.003 inch. Some waves had smaller lengths of about 2 inches, with trough-to-crest heights of about 0.002 inch. In general, the maximum gage-measured waviness was ±0.001 inch per linear inch at the joints and ±0.005 inch per linear inch elsewhere. Waviness also proved identical from one shell segment to the next, indicating that the waviness was in the die and that little variation occurred from one segment to another. These measurements were conducted only on the first shell; it is believed that the waviness of the final test shell would be essentially identical since the same die was used.

Figure 37 shows the sting-mounted model in the wind tunnel at Northrop. The model tests proceeded very quickly; the model did not have to be smoothed, nor was it necessary to change its surface in any way. These results indicated that surface roughness and waviness were not a problem under the test conditions used.

A possible prototype torpedo using boundary-layer control is shown in Fig. 38. Here the standard torpedo components are placed inside a pressure-protected hull with a duct of about 1/4 inch between it and a surrounding porous shell. This duct widens near the tail so that an internal pump might be included. As shown in Fig. 38, the pump would also be used to provide propulsive thrust. A very small pump could be used because thrust requirements are low and the velocity increase of the water is high. An additional feature is that the shell can clog by a factor of two, while the suction rate will remain essentially unchanged. This is because only about 5% of the pump power is used for suction through the shell. Doubling this value does not appreciably change the pump speed or flow rate.

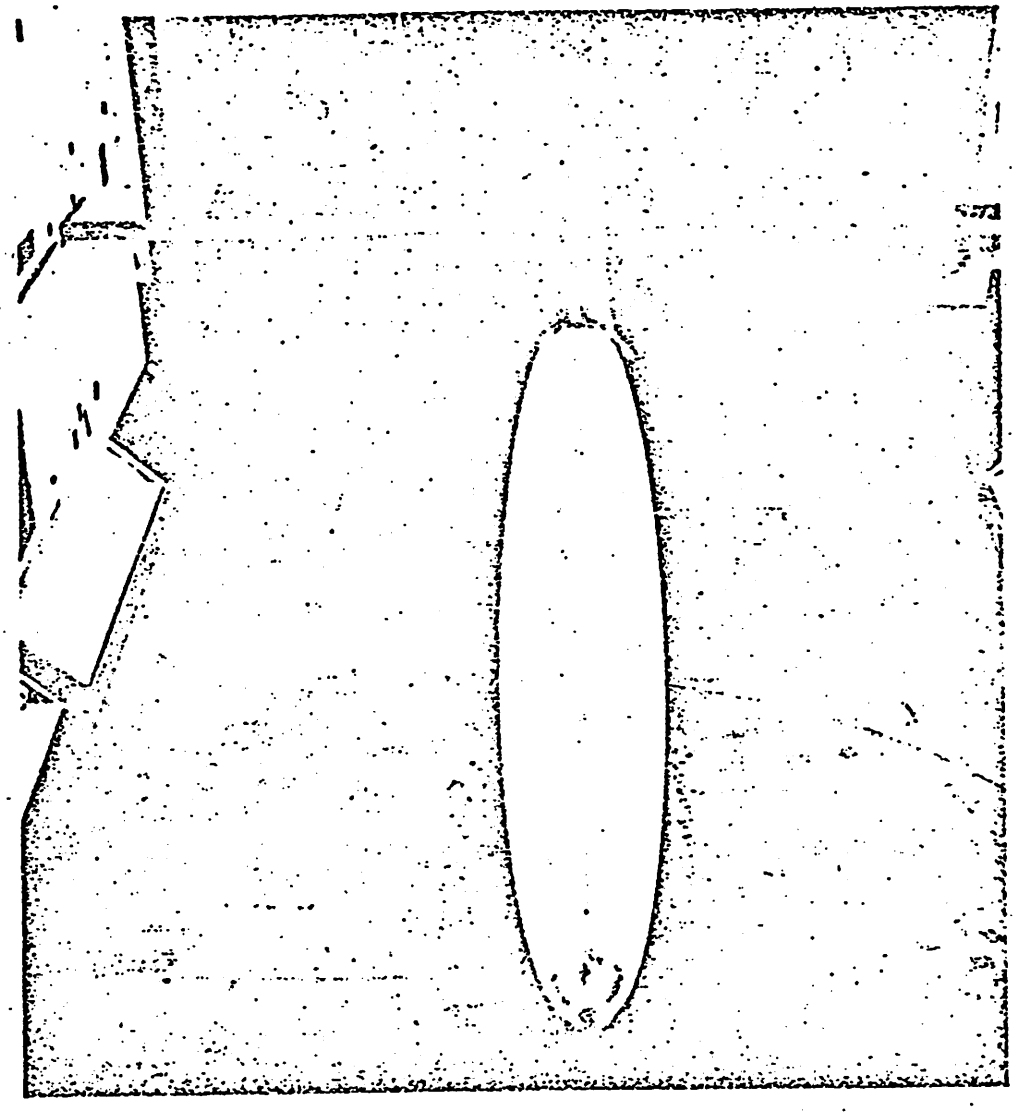

FIG. 37. NOTS Porous Model Mounted in Northrop Wind Tunnel.

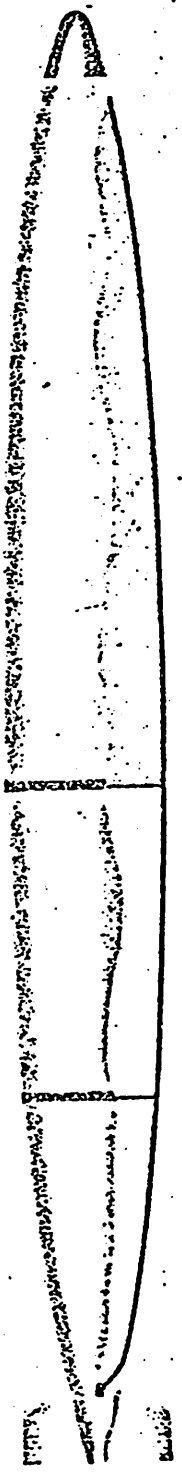

FIG. 38. A Possible Prototype Torpedo Using Boundary-Layer Control.

Appendix B

TEST SETUP AND DATA PROCESSING

The tests were conducted in the 7-by-10-foot low-turbulence Norair wind tunnel, which has a noise and vibration R_ℓ limit of about 11 to 12×10^6, based on the NOTS model length. The wake drag of the model was measured by means of the six wake rakes shown in Fig. 39. The model was internally divided into three suction chambers, each connected to pipes passing through the Northrop floor-supported sting by way of calibrated flow-measuring nozzles to a suction box. The suction rate was controlled by remotely-operated needle valves.

There were at least two static-pressure pickups in each of the three chambers, with at least one near the shell and another near the chamber outlet. These lines passed through the sting to a bank of U-tube manometers.

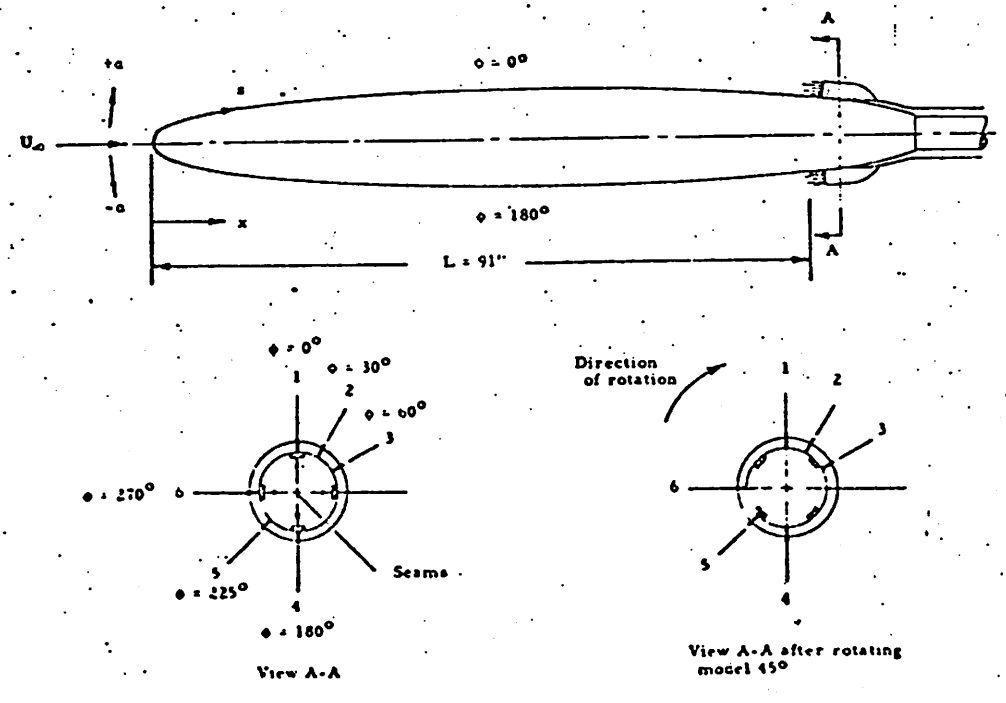

FIG. 39. Location of Wake Rakes and Body Seams.

The wake rakes consisted of multiple-total head tubes located at different heights from the skin, the first being as close to the skin as possible. Each rake had two static-pressure pickups located where they would not interfere with the flow past the other rakes. These tubes were externally attached to the sting and connected to the manometer bank.

The manometer banks were photographed and the resulting data, on 70-mm film, were partially reduced by a film-reading machine. They were then put into a form that could be used on punched cards in an IBM 7090 digital computer. The final data reduction used the same computer program, with minor changes, that Northrop personnel had created for their model.

Appendix C

THEORETICAL BOUNDARY-LAYER CALCULATIONS

by

A. G. Fabula

Several laminar-flow boundary-layer analyses of varying degrees of refinement have been made on the Reichardt ovoid body shape used in these tests. In all these theoretical calculations, only steady, incompressible, axisymmetric flow has been considered.

The writer's laminar-boundary-layer calculations for the Reichardt ovoid were based on the approximate, one-parameter, modified Schlichting analysis (Ref. 10). They served mainly to confirm that, in the intended towing-tank tests, a typical anticipated suction coefficient of $C_Q = 3 \times 10^{-4}$ for uniform suction over the porous shell would, in theory, suffice to stabilize the boundary layer for an intended maximum speed of 45 knots, assuming that shell waviness, shell-surface roughness, and freestream (i.e., tank) turbulence were unimportant.

The analyses were as follows. With the calculated distribution of Schlichting's velocity profile, Shape Parameter K versus surface distance from the stagnation point, the corresponding critical-thickness Reynolds number for neutral stability, R_{θ_c}, was obtained from Ref. 11. Therefore, suction was assumed to stabilize the boundary layer as long as $R_\theta < R_{\theta_c}$. For the high Reynolds numbers considered for the towing-tank tests, there was a short interval of instability ahead of the porous shell's leading edge. However, by applying Granville's method (Ref. 12) to predict the separation of the neutral-stability and transition points (for the no-suction case), it was concluded that boundary-layer stabilization by suction would result because the no-suction transition point would be well beyond the leading edge of the porous shell.

In later calculations, W. G. Reller and W. B. Giles of the General Electric Co. also considered the NOTS body with its solid nose, using a more accurate analysis based on their extension of M. R. Head's method to axisymmetric boundary layers. The results for uniform suction indicated somewhat greater stability than did the Schlichting analysis. Reller and Giles also calculated the optimum suction distribution over the porous shell for the NOTS body with a body-length Reynolds number $R_\ell = 33 \times 10^6$. Over most of the porous shell, the resultant optimum local suction coefficient was between 1.25 and

0.75×10^{-4}. This is similar to the result of Wieghardt (Ref. 13) for a solid-nose ellipsoid, also of 8:1 fineness ratio, with $R_\ell = 8 \times 10^6$. The fact that the experimental optimum C_Q in the present tests is typically about 2×10^{-4} is not explained, but may be due to the theory, which is basically two-dimensional, or to a variety of experimental conditions, such as surface waviness, variations in shell permeability, and tunnel turbulence. However, it is notable that Norair's slotted model, when tested under the same tunnel conditions, also had an optimum C_Q of 2×10^{-4}, and unofficial results for the Ames tests show nearly the same value. Thus refinement of the neutral-stability theory for bodies of revolution would be worthwhile.

To date, the most detailed and refined theoretical boundary-layer calculations for a Reichardt ovoid shape have been made at Northrop in connection with the Norair study of laminar-flow control by means of suction through slots on an 8:1 ovoid 18 inches in diameter (compared with a 12.75-inch diameter for the porous NOTS model). The Norair calculations, based on machine computations using the Raetz method (Ref. 14), were used to determine slot spacing and to allow a detailed comparison of theoretical and experimental boundary-layer profiles at the wake rakes (Ref. 7). Another machine-computation program for laminar boundary-layer calculations was developed by the Douglas Aircraft Co., Inc., based upon the Hartree-Womersly method. Example calculations for the NOTS Reichardt ovoid with and without suction have also been made (Ref. 15).

Detailed calculations could be performed now on the porous NOTS model to compare theoretical laminar-flow profiles with the experimental boundary-layer profiles from the rake measurements, but it is clear from the experimental results already given that the comparison would be of limited interest. Furthermore, the main usefulness of theoretical calculations of this sort is for future work, where optimum suction distributions for more torpedolike shapes may have to be considered. Such work is now under way at Norair.

REFERENCES

1. Lang, T. G. "New Torpedo Concepts," Torpedo Quarterly. U. S. Naval Ordnance Test Station, China Lake, Calif., May 1957. (NAVORD Report 5572, NOTS 1768), CONFIDENTIAL.

2. U. S. Naval Ordnance Test Station. Control of Torpedo Boundary Layers by Suction, by T. G. Lang and J. D. Brooks. China Lake, Calif., NOTS, 30 April 1959. (NAVORD Report 6536, NOTS TP 2231.)

3. ———. Torpedo Drag Reduction (U), by T. G. Lang. China Lake, Calif., NOTS, 21 May 1959. (NAVORD Report 6451, NOTS TP 2164), CONFIDENTIAL.

4. ———. Investigations of Torpedo Drag Reduction at the Naval Ordnance Test Station (U), by T. G. Lang. China Lake, Calif., NOTS, 10 March 1961. (NAVWEPS Report 7638, NOTS TP 2651), CONFIDENTIAL.

5. ———. A Feasibility Study of Torpedoes With Boundary-Layer Control (U), by J. D. Bascom. China Lake, Calif., NOTS, 20 June 1961. (NAVWEPS Report 7748, NOTS TP 2715), CONFIDENTIAL.

6. Boundary Layer and Flow Control, Its Principles and Application (Vol. 1 and 2), G. V. Lachman, ed. New York, Pergamon, 1961.

7. Northrop Corp., Norair Div. Investigation of a Reichardt Body of Revolution With Low Drag Suction in the Norair 7-by 10-Foot Tunnel (U), by L. W. Gross. Hawthorne, Calif., Northrop, December 1962. Report NOR-62-126 (BLC-143), SECRET.

8. Munzner, H., and H. Reichardt. Rotationally Symmetric Source-Sink Bodies With Predominantly Constant Pressure Distributions. (Nov. 1944.) Armament Research Establishment Translation No. 1/50 by A. H. Armstrong, April 1950.

9. Douglas Aircraft Co., Inc. Exact Solution of the Neumann Problem; Calculation of Non-Circulatory Plane and Axially Symmetric Flows About or Within Arbitrary Boundaries, by A. M. O. Smith and J. Pierce. Santa Monica, Calif., Douglas, April 1958. (Report ES 26988.)

10. National Advisory Committee for Aeronautics. Theoretical Distribution of Laminar-Boundary-Layer Thickness, Boundary-Layer Reynolds Number and Stability Limit, and Roughness Reynolds Number for a Sphere and Disk in Incompressible Flow, by Neal Tetervin. Washington, NACA, September 1958. (NACA Report TN 4350.)

11. ———. A Study of the Stability of the Laminar Boundary Layer as Affected by Changes in the Boundary-Layer Thickness in Regions of Pressure Gradient and Flow Through the Surface, by N. Tetervin and D. A. Levine. Washington, NACA, August 1952. (NACA Report TN 2752.)

12. David Taylor Model Basin. The Calculation of the Viscous Drag of Bodies of Revolution, by P. S. Granville. Washington, DTMB, July 1953. (DTMB Report 849.)

13. Wieghardt, K. Zur Berechnung ebener und drehsymmetrischer Grenzschicten mit kontinuerlicher Absangung. Ingenieur Archiv, Band XX11 (1954), pp. 368 - 377.

14. Northrop Corp., Norair Div. A Method of Calculating Three-Dimensional Laminar Boundary Layers of Steady Compressible Flows, by Gibbs S. Raetz. Hawthorne, Calif., Northrop, December 1957. (BLC-114.)

15. Douglas Aircraft Co., Inc. Solution of the Incompressible Laminar Boundary Layer Equations, by A. M. O. Smith and D. W. Clutter. Santa Monica, Calif., Douglas, 29 July 1961. (Report ES 40446.)

INITIAL DISTRIBUTION

11 Chief, Bureau of Naval Weapons
- DLI-31 (2)
- R-12 (1)
- RAAD-3 (1)
- RRRE (1)
- RRRE-4 (1)
- R-5 (1)
- RU (1)
- RUTO (1)
- RUTO-32 (2)

7 Chief, Bureau of Ships
- Code 106 (1)
- Code 335 (1)
- Code 421 (2)
- Code 442 (2)
- Code 644 (1)

1 Chief of Naval Operations

4 Chief of Naval Research
- Code 104 (1)
- Code 429 (1)
- Code 438 (1)
- Code 466 (1)

7 David W. Taylor Model Basin
- Code 142 (1)
- Code 500 (1)
- Code 513 (1)
- Code 526 (1)
- Code 580 (1)
- Code 800 (1)

1 Naval Academy, Annapolis (Librarian)

1 Naval Air Development Center, Johnsville

1 Naval Aircraft Torpedo Unit, Quonset Point

1 Naval Civil Engineering Laboratory, Port Hueneme (Code L54)

1 Naval Engineering Experiment Station, Annapolis

2 Naval Ordnance Laboratory, White Oak
- Library Division, Desk HL (1)

1 Naval Postgraduate School, Monterey (Library, Technical Reports Section)

2 Naval Research Laboratory
- Code 5550 (1)

1 Naval Torpedo Station, Keyport (Quality Evaluation Laboratory, Technical Library)

1 Naval War College, Newport (Institute of Naval Studies)
1 Naval Weapons Laboratory, Dahlgren
2 Naval Weapons Services Office
1 Navy Electronics Laboratory, San Diego
1 Navy Mine Defense Laboratory, Panama City
1 Navy Underwater Sound Laboratory, Fort Trumbull
1 Office of Naval Research Branch Office, Pasadena
1 Air Force Office of Scientific Research (Mechanics Division)
1 Director of Defense (R & E) (Office of Fuels, Materials and Ordnance, Bayard Belyea)
20 Defense Documentation Center (TISIA-1)
1 Committee on Undersea Warfare
1 Maritime Administration (Coordinator for Research)
1 National Bureau of Standards (Fluid Mechanics Section, Dr. G. Schubauer)
2 National Science Foundation
Director, Engineering Sciences Division (1)
1 Scientific and Technical Information Facility, Bethesda (NASA Representative (S-AK/DL)
2 Aerojet-General Corporation, Azusa, Calif., via BWR
Librarian (1)
J. Levy (1)
1 Airesearch Manufacturing Company, Los Angeles (Dr. B. R. Parkin)
1 Applied Physics Laboratory, University of Washington, Seattle
1 Baker Manufacturing Company, Evansville, Wisc.
3 California Institute of Technology, Pasadena (Engineering Division)
Dr. C. B. Millikan (1)
Dr. M. S. Plesset (1)
Dr. V. A. Vanoni (1)
1 Clevite Ordnance, Cleveland
1 Cornell Aeronautical Laboratory, Inc., Buffalo (Department 410)
1 Cornell University, Graduate School of Aeronautical Engineering, Ithaca (Library)
2 Davidson Laboratory, Stevens Institute of Technology, Hoboken, N. J.
A. Suarez (1)
Dr. J. Breslin (1)
1 Douglas Aircraft Company, Inc., Long Beach, Calif. (Aerodynamics Section)
1 Eastern Research Group, New York City
1 Electric Boat Division, General Dynamics Corporation, Groton, Conn. (D. D. Walden)
1 General Dynamics/Astronautics, Space Science Laboratory, San Diego
3 General Dynamics/Convair, San Diego
Engineering Library (1)
Hydrodynamics Laboratory (1)
Scientific Research Laboratory (1)
1 General Electric Company, Defense Electronics Division, Pittsfield, Mass. (Engineering Librarian)
1 General Electric Company, Johnson City, N. Y. (Light Military Electronics Department, Armament & Control Products Section, Library)

2 Gibbs and Cox, Inc., New York City
Dr. S. Hoerner (1).
Library (1)
1 Grumman Aircraft Engineering Corporation, Bethpage, N. Y.
(Library)
1 Hudson Laboratories, Columbia University, Dobbs Ferry, N. Y.
1 Hydronautics, Inc., Rockville, Md.
1 Lockheed Aircraft Corporation, Burbank, Calif.
1 Lockheed Aircraft Corporation, Missiles and Space Division,
Palo Alto, Calif. (R. W. Kermeen)
2 Massachusetts Institute of Technology, Cambridge
Department of Civil Engineering (1)
Department of Naval Architecture and Marine Engineering (1)
1 North American Aviation, Inc., Los Angeles (Technical Library,
Department 56)
2 Ordnance Research Laboratory, Pennsylvania State University,
State College, via RRINM (Garfield Thomas Water Tunnel)
1 The Bendix Corporation, Bendix Pacific Division, North Hollywood
1 University of California, San Diego, Scripps Institution of Oceanography, Marine Physical Laboratory, San Diego
1 Westinghouse Electric Corporation, Baltimore (Engineering Librarian)
1 Westinghouse Research Laboratories, Pittsburgh (Arthur Nelkin)
1 Woods Hole Oceanographic Institution, Woods Hole, Mass.
5 British Joint Services Mission (Navy Staff), via BuWeps (DSC-32)
2 Defence Research Member, Canadian Joint Staff (W), via BuWeps
(DSC-32)

ABSTRACT CARD

U. S. Naval Ordnance Test Station
Wind-Tunnel Tests on a Porous Body With Suction (U), by T. G. Lang and H. V. L. Patrick. China Lake, Calif., NOTS, December 1964. 36 pp. (NAVWEPS Report 8528, NOTS TP 3529), CONFIDENTIAL.

Card
UNCLASSIFIED

(Over)
1 card, 4 copies

U. S. Naval Ordnance Test Station
Wind-Tunnel Tests on a Porous Body With Suction (U), by T. G. Lang and H. V. L. Patrick. China Lake, Calif., NOTS, December 1964. 36 pp. (NAVWEPS Report 8528, NOTS TP 3529), CONFIDENTIAL.

Card
UNCLASSIFIED

(Over)
1 card, 4 copies

U. S. Naval Ordnance Test Station
Wind-Tunnel Tests on a Porous Body With Suction (U), by T. G. Lang and H. V. L. Patrick. China Lake, Calif., NOTS, December 1964. 36 pp. (NAVWEPS Report 8528, NOTS TP 3529), CONFIDENTIAL.

Card
UNCLASSIFIED

(Over)
1 card, 4 copies

U. S. Naval Ordnance Test Station
Wind-Tunnel Tests on a Porous Body With Suction (U), by T. G. Lang and H. V. L. Patrick. China Lake, Calif., NOTS, December 1964. 36 pp. (NAVWEPS Report 8528, NOTS TP 3529), CONFIDENTIAL.

Card
UNCLASSIFIED

(Over)
1 card, 4 copies

UNCLASSIFIED

NAVWEPS Report 8528

ABSTRACT. Tests were performed in a 7-by-10-foot wind tunnel to determine the drag characteristics of a full-scale, porous-shelled torpedo model with suction applied to three internal chambers. The model was a Reichardt body of revolution having a nearly uniform pressure distribution with a fineness ratio of 8:1 and a diameter of 12 3/4 inches. The drag was measured by means of six boundary-layer rakes located 91 inches from the nose. The test data were obtained at Reynolds numbers up to 12×10^6, the turbulence limit of the wind tunnel.

NAVWEPS Report 8528

ABSTRACT. Tests were performed in a 7-by-10-foot wind tunnel to determine the drag characteristics of a full-scale, porous-shelled torpedo model with suction applied to three internal chambers. The model was a Reichardt body of revolution having a nearly uniform pressure distribution with a fineness ratio of 8:1 and a diameter of 12 3/4 inches. The drag was measured by means of six boundary-layer rakes located 91 inches from the nose. The test data were obtained at Reynolds numbers up to 12×10^6, the turbulence limit of the wind tunnel.

NAVWEPS Report 8528

ABSTRACT. Tests were performed in a 7-by-10-foot wind tunnel to determine the drag characteristics of a full-scale, porous-shelled torpedo model with suction applied to three internal chambers. The model was a Reichardt body of revolution having a nearly uniform pressure distribution with a fineness ratio of 8:1 and a diameter of 12 3/4 inches. The drag was measured by means of six boundary-layer rakes located 91 inches from the nose. The test data were obtained at Reynolds numbers up to 12×10^6, the turbulence limit of the wind tunnel.

NAVWEPS Report 8528

ABSTRACT. Tests were performed in a 7-by-10-foot wind tunnel to determine the drag characteristics of a full-scale, porous-shelled torpedo model with suction applied to three internal chambers. The model was a Reichardt body of revolution having a nearly uniform pressure distribution with a fineness ratio of 8:1 and a diameter of 12 3/4 inches. The drag was measured by means of six boundary-layer rakes located 91 inches from the nose. The test data were obtained at Reynolds numbers up to 12×10^6, the turbulence limit of the wind tunnel.

UNCLASSIFIED

UNCLASSIFIED